A NON-CANONICAL ROLE FOR P107 IN MUSCLE STEM CELL FATE DECISIONS

JUSTIN HSIUNG

A THESIS SUBMITTED TO THE FACULTY OF GRADUATE STUDIES IN PARTIAL FULFILLMENT OF THE REQUIREMENTS FOR THE DEGREE OF MASTER OF SCIENCE

GRADUATE PROGRAM IN BIOLOGY

YORK UNIVERSITY
TORONTO, ONTARIO
DECEMBER 2023

Abstract

The regenerative potential of skeletal muscle is attributed to the presence of resident muscle stem cells known as satellite cells (SCs). After activation SCs have two fates, either to differentiate into new muscle or self-renew to replenish their population. Dysregulation in favor of one outcome over the other has been implicated in loss of muscular regenerative capacity. Mitochondrial metabolism has recently emerged as a regulator of SC fate decisions. We uncovered a non-canonical mitochondrial role for retinoblastoma-like protein 1 (Rbl1, p107) in manipulating fate decisions through its effect on mitochondrial dynamics. We find that in the absence of mitochondrially localized p107, SCs display a higher rate of self-renewal, while also exhibiting higher mitochondrial connectivity. This was associated with increases in the mitochondrial fusion protein OPA1, as well as a loss in cellular acetylation. Taken together, these findings suggest that non-canonical p107 function in SCs controls their cell fate decisions.

Acknowledgements

I would first like to thank my supervisor, **Dr. Anthony Scimè,** for giving me this amazing opportunity two years ago. Without your constant guidance and mentorship, I would not be where I am today. Your passion for research truly inspired me to pursue my own path in science, and your constant motivation and encouragement did not go unnoticed. I appreciate the countless number of hours you have put into reviewing my work and helping me improve not only my laboratory skills, but my writing as well. Thank you so much for believing in me, giving me a chance, and helping me throughout my academic journey.

I would also like to thank **Dr. Chun Peng** for being part of my supervisory committee. Thank you for showing interest in my research throughout the years. I would also like to thank **Dr. Tara Haas** for your regular insight and suggestions in our research projects, as well as allowing us to borrow reagents at a moment's notice.

To all my lab mates, volunteers, and everyone that came through the lab over the past two years, thank you for always making the lab such an inviting place to be. I would like to thank my lab mates **Lucas**, **Vicky**, and **Mark** for their support and guidance, and for taking the time to teach me without hesitation. Moreover, thank you for always being willing to help with my experiments, I could never have done it without you all.

Most importantly, I would like to thank my **family** for always being with me throughout my journey and encouraging me to take this opportunity. Without the constant support at home, I probably would not have made it to where I am today. I hope to make you all proud by achieving my dreams.

Table of Contents

List of Figures

Chapter 1:

Chapter 4:

Chapter 5:

List of Abbreviations

SC	Satellite cell
Pax7	Paired box transcription factor 7
MyoD	Myoblast determination protein 1
Myf5	Myogenic factor 5
mRNA	Messenger ribonucleic acid
DMD	Duchenne muscular dystrophy
mTORC	Mammalian target of rapamycin complex
NAD^+	Nicotinamide adenine dinucleotide
NADH	Reduced nicotinamide adenine dinucleotide
LDH	Lactate dehydrogenase
TCA	Tricarboxylic acid cycle
ATP	Adenosine triphosphate
$FADH_2$	Flavin adenine dinucleotide
ETC	Electron transport chain
UQ	Ubiquinone
CytC	Cytochrome C
CoA	Coenzyme A
ADP	Adenosine diphosphate
ROS	Reactive oxygen species
mtDNA	Mitochondrial dideoxyribonucleic acid
Mfn1/2	Mitofusin 1/Mitofusin 2
Drp1	Dynamin related protein 1

OPA1	Optic atrophy gene 1
OMA1	*m*-AAA protease 1
YME1L	Yeast mitochondrial escape 1-like protein
Sirt(1-7)	Sirtuin(1-7)
Rbl1, p107	Retinoblastoma like protein 1
Rb, Rb1	Retinoblastoma protein
Rbl2, p130	Retinoblastoma like protein 2
p107KO	p107 genetically deleted
MEF	Murine embryonic fibroblast
MPC	Myogenic progenitor cell
WT	Wildtype
SDS-PAGE	Sodium dodecyl sulfate polyacrylamide gel electrophoresis
MTS	Mitochondrial targeting sequence

CHAPTER 1

LITERATURE REVIEW

1.1 Satellite cells

Skeletal muscle is one of the largest metabolic organs in the body, and is required for physical motion (Tieland et al., 2018). Composed of thousands of multinucleated myofibers, each muscle works together simultaneously to achieve contraction and relaxation events, creating coordinated movements (Goodman et al., 2015). In addition to movement, skeletal muscle serves a vital role in glucose and fatty acid metabolism, due to its proportion in body mass, variable metabolic rate, and ability for metabolic and mitochondrial adaptation (Hickson et al., 1977; McFarlan et al., 2012). As a critical organ system for both movement and metabolism, skeletal muscle must be able to undergo regeneration to compensate for changes in muscle demand, everyday use, and recovering from traumatic injury.

The regenerative potential of skeletal muscle is made possible through the presence of muscle resident adult myogenic stem cells termed satellite cells (SCs) (Mauro, 1961; Sousa-Victor et al., 2022). Residing between the basal lamina and sarcolemma, they were originally believed to be dormant cells involved in muscular regeneration (Mauro, 1961). This was confirmed almost 10 years later, with research revealing that SCs are precursors to the myoblast cells that were responsible for skeletal muscle regeneration and maintenance (Moss and Leblond, 1970; Reznik, 1969). SCs make up about 2% to 10% of all muscular nuclei, and their location allows for the rapid response to signals in the surrounding microenvironment (Dumont et al., 2015a). As with other stem cells, SCs can undergo self-renewal to replenish their population or differentiate to add new nuclei to already existing myofibers, or create new myofibers (Yin et al., 2013). The self-renewal

function of SCs is critical for muscle fiber regeneration, as losses in the SC population can lead to poor muscle regeneration.

Under normal physiological conditions, in the absence of a stressor such as injury, SCs remain in a dormant state of quiescence. While not actively dividing, they are metabolically active, though require little energy (Sousa-Victor et al., 2022; Bhattacharya and Scimè, 2020). Upon receiving signals from a stressor, SCs undergo the process of activation, which draws them out of quiescence and starts their proliferation to generate or repair myofibers (Dumont et al., 2015a). During this process, some of the newly generated SCs will self-renew, rather than differentiate, replenishing the stem cell population. Once regeneration is complete, the SC population should be restored, and the muscle repaired through SC differentiation (Sousa-Victor et al., 2022).

The delicate balance between self-renewal and differentiation is critical, as tipping the balance in either direction could result in muscular disorders and impaired regeneration, such as what is observed in muscular dystrophies (Chang et al., 2016). For example, a study by Brun et al. found that deletion of GLI3 causes SC preference for self-renewal (Brun et al., 2022). Although this is able to generate hyperplasia in the stem cell pool, upon repeated injury and regeneration cycles, it was found the GLI3 deleted muscles generated smaller muscle fibers (Brun et al., 2022). Conversely, an increase in commitment to the differentiation pathway also causes impaired regeneration. The Notch signaling pathway is required for maintaining quiescence and self-renewal properties of SCs, with its downregulation being associated with activation and differentiation (Giofsidi et al., 2022). Upon disruption of Notch nuclear factor RBP-J, it was found that murine SCs proceeded to lose the ability to self-renew, effectively diminishing their population (Bjornson, et al., 2012). The lack of Notch signaling caused the activated SCs to

instantly commit to differentiating and fusing to existing myofibers, rather than self-renewing or proliferating to repair the muscular insult (Bjornson, et al., 2012).

1.2 Satellite cell transitions

SC fates can be tracked by the expression of various proteins (Sousa-Victor et al., 2022). Quiescence and self-renewal are marked by the exclusive expression of paired box transcription factor 7 (Pax7), while activated and proliferating SCs express both Pax7, as well as proteins involved in the myogenic differentiation pathway such as myoblast determination protein 1 (MyoD), and myogenic factor 5 (Myf5) (Seale et al., 2000; Cornelison and Wold, 1997). SCs committed to differentiate lose Pax7 expression entirely and eventually exclusively express muscle differentiation markers (Zammit, 2017). Conversely, those that self-renew to become part of the quiescent SC pool lose MyoD and Myf5 protein expression. Therefore, using the different markers during the SC transitions, one can follow SCs from quiescence (Pax7+/MyoD-), activation and proliferation (Pax7+/MyoD+), and commitment to the differentiation pathway (Pax7-/MyoD+) (**Fig 1.1**) (Yin et al., 2013; Dumont et al., 2015a).

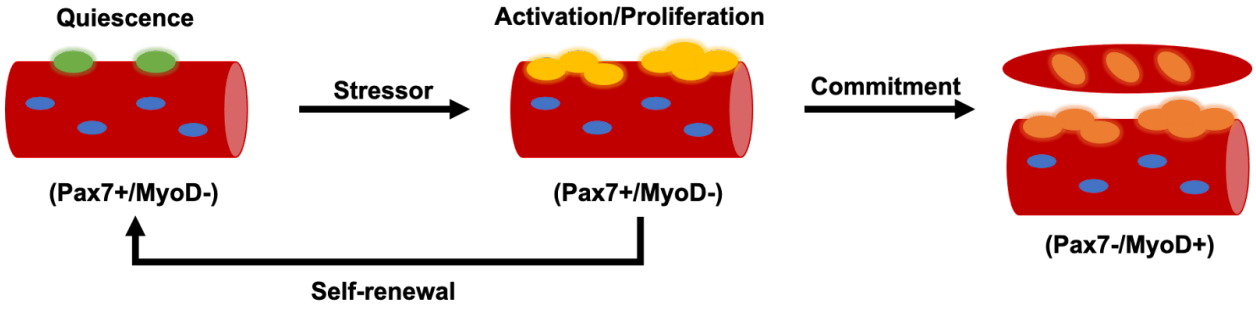

Fig 1.1. Schematic of SC transitions and the markers associated with each state. SCs are normally found in a quiescent state on the myofiber between the basal lamina and sarcolemma. Upon introduction of a stimulus, they activate and begin proliferation to generate a sufficient population for muscular regeneration. SCs then differentiate to generate new myofibers, while a small portion of activated SCs return to quiescence to replenish the SC pool.

The activation of SCs from quiescence is a rapid process due to storage of Myf5 and MyoD messenger ribonucleic acids (mRNAs) in cytoplasmic granules (Crist et al., 2012). The mRNA found in the granules are transcribed while the cell is in quiescence, and rapidly dissociate upon activation, releasing MyoD and Myf5 mRNA directly into the cytosol for translation (Crist et al., 2012; Ribeiro et al., 2019). This process skips the need to transcribe mRNAs to initiate the myogenic pathway, facilitating faster progress towards activation. After activation, cells will divide either symmetrically, or asymmetrically. In symmetric divisions two daughter cells with identical fates are generated. However, SCs that have not expressed Myf5 at any point during development can also undergo asymmetric divisions, where each daughter cell results in a different fate decision, which is self-renewal or differentiation (Kuang et al., 2007; Dumont et al., 2015b). During an asymmetric division, it was found that the division occurred in an apicobasal fashion, with one daughter SC facing the muscle fiber, and the other towards the basement membrane. For symmetric divisions, it occurs parallel along the muscle fiber (Kuang et al., 2007; Dumont et al., 2015b). While disruptions to SC fate decisions can cause muscular disorders, imbalances in division type can also affect muscular health. In Duchenne muscular dystrophy (DMD), the lack of dystrophin causes a loss in SC polarity within the myofiber, which disrupts the ability for SCs to divide asymmetrically, leading to a loss in myogenic progenitors (Chang et al., 2018; Dumont et al., 2015b).

1.3 Satellite cell heterogeneity

Studies have shown that SCs exist as a heterogeneous population. They exist in a spectrum of quiescent states, which are based on the timing for initiation of activation (Rodgers et al., 2014). For example, upon muscular injury, SCs at the site of injury undergo normal activation and

differentiation, but distal SCs not involved in the injury become primed for activation, entering a state termed ‘G-alert’ (Rodgers et al., 2014). While not out of quiescence as they are not actively dividing, G-alert SCs are marked by triggering the mTORC pathway and grow larger in size relative to normally quiescent SCs (Rodgers et al., 2014). These G-alert SCs have enhanced entry into the cell cycle and display faster rates of muscular regeneration than non-alerted SCs (Rodgers et al., 2014).

Also, single-cell RNA sequencing of quiescent SC populations show varying levels of Pax7, metabolic, and self-renewal related genes such as Notch-2 (Dong and Doles, 2017; Yartseva et al., 2020). Dong and Doles found that individual SCs had varying levels of gene expression for various metabolic pathways and processes, such as carbohydrate or lipid metabolism, which can influence their depth of quiescence (Dong and Doles, 2017; Rodgers et al., 2014; van Velthoven and Rando, 2019). Yartseva et al. demonstrated that a subpopulation of quiescent SCs display higher rates of Notch-2 signaling which persists through activation and causes a preference for self-renewal (Yartseva et al., 2020). Single-cell RNA sequencing of human SCs also describes a population of quiescent SCs enriched in proliferation and myogenic program genes, indicating that these SCs have lower depths of quiescence than their counterparts (De Micheli et al., 2020).

Rocheteau et al., observed that quiescent SCs can be discriminated by their level of Pax7 expression (Rocheteau et al., 2011). The Pax7 high population exists in a state of deeper quiescence, displaying a lower metabolic rate and taking longer to execute the first mitosis event after activation. However, its cycling time after the initial mitosis event remains on par with the rest of the SC pool. Conversely, the Pax7 low SCs exist in a shallower quiescence, displaying a phenotype more primed for activation and myogenic commitment (Rocheteau et al., 2011).

In addition to differing depths of quiescence, there exists a subpopulation of SCs composing roughly 10% of the total SC pool that have never expressed Myf5 in their development (Kuang et al., 2007). Though Myf5- SCs can divide symmetrically, they can also divide asymmetrically, giving rise to one daughter cell that is Pax7+/Myf5+, and one that is Pax7+/Myf5- (Kuang et al., 2007; Yin et al., 2013). It is thought that the Myf5- SCs serve to replenish the SC pool through their symmetric divisions but contribute to regeneration through asymmetric divisions (Kuang et al., 2007; Relaix et al., 2021).

1.4 Glycolysis and oxidative phosphorylation

Cellular metabolism can be classified into two primary categories being either oxidative, which generates ATP in the mitochondria, or non-oxidative, which generates ATP in the cytoplasm. Glycolysis, in the cytosol, creates a net of two ATP molecules, as well as producing nicotinamide adenine dinucleotide (NADH) and potentially substrates that can be used for nucleotide, lipid or amino acid production (Lunt and Heiden, 2011). The NADH generated from glycolysis is either shuttled into the mitochondria via the malate-aspartate shuttle to be used as a reducing equivalent in oxidative phosphorylation (Oxphos) or used in the lactate dehydrogenase (LDH) catalyzed reaction that turns pyruvate, the end product of glycolysis, into lactate (DeBerardinis et al., 2008; Kane, 2014). This reaction oxidizes NADH back into NAD^+, which occurs in the absence of oxygen when the mitochondria is unable to act as a NADH recycler. Otherwise, in the presence of oxygen, pyruvate is turned into acetyl-CoA through pyruvate dehydrogenase that is fed into the mitochondrial tricarboxylic acid cycle (TCA) (DeBerardinis et al., 2008; Martinez-Reyes and Chandel, 2020) (**Fig. 1.1**). While the lactate pathway is usually

reserved for anaerobic metabolism, the pathway also occurs when there is a rapid demand for ATP, as glycolysis generates ATP at a faster rate than Oxphos (Lunt and Heiden, 2011).

Oxphos takes place in the mitochondria, which are double membraned organelles that have an inner and outer membrane, with the inner membrane creating folds called cristae (Nielsen et al., 2017; Leduc-Gaudet et al., 2021). The space enveloped by the inner membrane is referred to as the mitochondrial matrix, and the space between the outer and inner membrane is the intermembrane space. Mitochondria are considered the bioenergetic hub of the cell, with the primary purpose of creating ATP. They accomplish this by oxidizing the reducing agents NADH

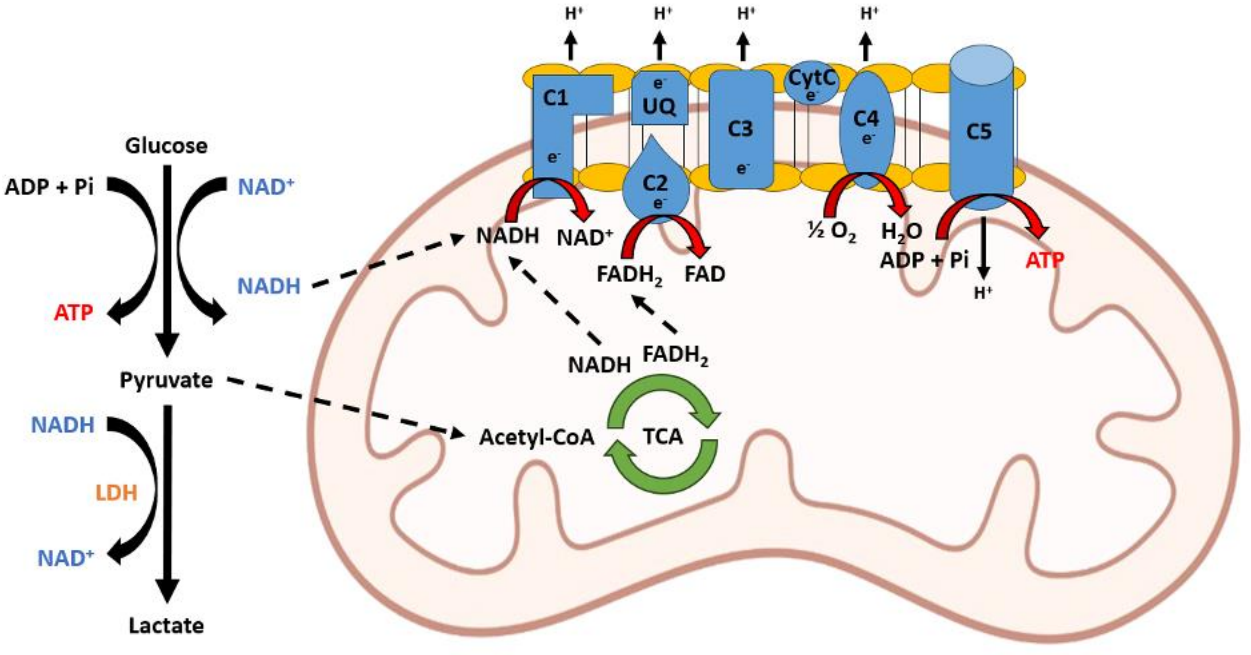

Figure 1.2. Diagram of glycolysis and Oxphos. Glucose is converted to pyruvate through glycolysis, which is then converted to acetyl-CoA and enters the TCA cycle. The TCA generates NADH and FADH, which along with NADH from glycolysis, is oxidized by the ETC and donates their electrons (e^-). Electrons are shuttled through complexes 1-5 (C1-C5) and transported through ubiquinone (UQ) and cytochrome C (CytC). Oxygen serves as the terminal electron acceptor in the chain, reducing into H_2O. This process causes protons to be pumped out of the mitochondrial matrix, and eventually return through C5, which converts ADP to ATP, generating energy through Oxphos. When Oxphos cannot occur, such as under conditions of hypoxia, pyruvate is converted into lactate using LDH, regenerating NAD^+ in the process.

and flavin adenine dinucleotide ($FADH_2$) in the electron transport chain (ETC) (Martinez-Reyes and Chandel, 2020). In the mitochondria $FADH_2$ and NADH are formed by the TCA cycle, which is a series of closed loop reactions that occur within the matrix (Arnold and Finley, 2022). Though glucose usually feeds the TCA cycle through acetyl-CoA, beta-oxidation of fatty acids and glutaminolysis also provide substrates for the TCA. This allows the mitochondria to use alternate fuel sources apart from glucose, such as fatty acids and amino acids (Martinez-Reyes and Chandel, 2020; Arnold and Finley 2022).

Electrons, from NADH and $FADH_2$, pass through the ETC where ATP is eventually produced. The ETC is composed of five complexes I to V, with an electron transporter termed ubiquinone between complexes I and III, and another termed cytochrome C between complexes III and IV (Martinez-Reyes and Chandel, 2020) (**Fig. 1.1**). As electrons pass through the ETC, protons are pumped into the intermembrane space from the matrix, creating an electrochemical gradient (Martinez-Reyes and Chandel, 2020). At the end of the chain, ATP synthase uses the proton gradient to produce ATP from ADP and phosphate, and the electron is transferred to a terminal electron acceptor in oxygen to form water (Martinez-Reyes and Chandel, 2020). This process may also generate reactive oxygen species (ROS) through leakage of electrons from complex I and III that does have signaling properties, though it is considered a waste product (Khacho et al., 2016).

The mitochondria is also unique in that it contains its own DNA independent of the nucleus. Mitochondrial DNA (mtDNA) is a small, double stranded, circular DNA molecule that is roughly 16.6 kb long in humans. It encodes for 13 polypeptides for subunits of the ETC, in addition to 2 rRNAs and 22 tRNAs for the translation of mtDNA mRNAs (Basu et al., 2020). mtDNA expression can directly affect mitochondrial ATP production, as a lack of ETC complex formation

can lead to lower Oxphos potential (Reinecke et al., 2009). As with nuclear DNA, the expression of mtDNA is regulated by various factors and pathways. Notably, the nucleus has control over mitochondrial gene expression as all regulatory proteins are encoded by the nucleus (Basu et al., 2020).

1.5 Satellite cell metabolism

SCs pass through various metabolic profiles which serve distinct purposes throughout each stage of quiescence, activation and proliferation, and differentiation (Latil et al., 2012; Ryall et al., 2015; Hori et al., 2019; Bhattacharya and Scimè, 2020). It has been shown that that the interplay between mitochondrial Oxphos and glycolysis plays an integral role in dictating stem cell fate decisions by influencing epigenetics or changing cellular ROS levels, which affects various downstream pathways (Ryall et al., 2015; Khacho et al., 2016; Lian et al., 2022; Bhattacharya and Scimè, 2020).

During quiescence, SCs are marked by a very low metabolic profile, favoring fatty acid beta-oxidation for energy production (Ryall et al., 2015; Relaix et al., 2021; Rocheteau et al., 2012, Baker et al., 2022). Upon activation and subsequent proliferation, SCs switch to glycolysis as the primary method of energy metabolism. This provides proliferating SCs with the macromolecules needed to meet their anabolic demands, as glycolytic intermediates can be processed into different biosynthetic pathways (Ryall et al., 2015; Folmes et al., 2012). As SCs begin differentiation, there is another dramatic shift in metabolism, with glycolysis making way for Oxphos, which was found to be critical for terminal differentiation (Seyer et al., 2006, 2011). Indeed, the inhibition of mitochondrial Oxphos and biogenesis was found to interfere with proper terminal differentiation, (Rochard et al., 2000; Zhang et al., 2020).

1.6 Mitochondrial dynamics

A factor that plays a crucial role in Oxphos regulation is mitochondrial network organization. Mitochondria are dynamic organelles, existing in a network that can bud off or elongate to alter their organization (Khacho et al., 2016). These processes are referred to as fission and fusion, and are often intertwined with mitophagy and biogenesis, as dysfunctional mitochondria break off from the network for degradation, and new mitochondria fuse with the existing network (Tilokani et al., 2018; Rafelski, 2013). The exact mechanism of how mitochondrial dynamics control cellular metabolism remains debated. It was found that when mitochondria are more interconnected, they can generate energy more efficiently than when disconnected (Mitra et al., 2009; Hoitzing et al., 2015, Gomes et al., 2011). It has also been established that mitochondrial fusion occurs to keep levels of ATP production consistent, especially during nutrient depletion (Gomes et al., 2011). During glucose restriction, the cell can no longer freely use glycolysis to generate energy and must switch to Oxphos for its primary energy production. Fusion is also believed to occur during times of cellular stress, which serves to protect mitochondria from degradation and autophagy (Gomes et al., 2011). Finally, it is thought that increasing the connectivity of mitochondria facilitates the 'mixing' of mitochondrial contents, allowing them to exchange mtDNA (Chen et al., 2010). This is believed to be useful for neutralizing any deleterious mutation in mtDNA affecting ETC complex formation, allowing other healthy networked mitochondria to compensate (Chen et al., 2010).

Control of mitochondrial dynamics lies in the three main fusion proteins: mitofusins 1 and 2 (Mfn1/2), and optic atrophy gene 1 (OPA1), with the main fission protein being dynamin related protein 1 (Drp1) (Mishra and Chan, 2016). Mitofusins 1/2 are responsible for the fusion of the outer mitochondrial membrane, while OPA1 mediates fusion of the inner membrane. Fusion

events are critical to maintaining mitochondrial and cellular health, and disruption to OPA1 causes cellular defects and dramatic mitochondrial fission (Chen et al., 2005). OPA1 is a GTPase and member of the dynamin gene family that has a role in maintenance of the ETC, cristae organization, and regulation of mitochondrial mediated apoptosis (Alvi and Fuhrmann, 2013; Cogliati et al., 2013). OPA1 is transcribed into eight different splice variants that encode for two general forms of OPA1, long (L-OPA1) or short (S-OPA1) (Song et al., 2007). These two forms complement each other, working cooperatively to perform mitochondrial fusion. It is currently understood that L-OPA1 is imported from the cytosol and embedded in the inner mitochondrial membrane, while S-OPA1 is a result of proteolytic cleavage of L-OPA1, freeing it from the membrane and creating a soluble protein (Ishihara et al., 2006; Tondera et al., 2009). Cleavage of L-OPA1 into its short form is facilitated by the two mitochondrial proteins, overlapping activities with the *m*-AAA protease 1 (OMA1) and yeast mitochondrial escape 1-like protein (YME1L). The former is activated under conditions of cellular stress, while the latter is continuously active to maintain basal levels of S-OPA1 (Anand et al., 2014). Both forms of OPA1 are essential to maintaining mitochondrial health, and their cooperation is critical in maintaining mitochondrial fusion activity. Excessive cleavage of L-OPA1 into S-OPA1 leads to mitochondrial fragmentation and predisposition to cell death (Anand et al., 2014; Tondera et al., 2009). Disproportionate cleavage is thought to be a control mechanism to attenuate fusion activity. Contrarily, Lee et al. showed that augmented levels of S-OPA1 can maintain mitochondrial cristae and energetics health, and that cells unable to create S-OPA1 are more sensitive to oxidative stress (Lee et al., 2020).

The mitochondrial fusion activity of OPA1 can also be controlled by post-translational acetylation. It was discovered that when acetylated at lysine site K^{926} and K^{931}, OPA1 displayed

significantly reduced GTPase activity, which is necessary for its fusion function (Samant et al., 2014; Alvi and Fuhrmann, 2013). This attenuation in activity resulted in mitochondrial fission, and the development of a disorganized mitochondrial network.

Mitochondrial fission is primarily controlled by the fission protein Drp1 (Tilokani et al., 2018). Mitochondrial fission, like fusion, is a critical cellular process that allows for normal cellular functioning. Waterham et al., found that a complete lack of Drp1 function led to a hyperfused mitochondrial network, which resulted in neonatal lethality (Waterham et al., 2007).

1.7 Mitochondrial dynamics and fate decisions

Recently, it has been demonstrated that OPA1 deficiency in SCs causes their depth of quiescence to be reduced to the point where they were found to be in the G-alert state (Baker et al., 2022). The inability to fuse mitochondria not only led to their altered quiescence but altered fate decisions in favour of commitment to differentiate over self-renewal. Chronic loss of OPA1 was found to cause significant mitochondrial metabolic dysfunction, reducing rates of ATP production and oxygen consumption (Baker et al., 2022). Additionally, it was found that short term loss of OPA1 resulted in fragmentation of the mitochondrial network (Baker et al., 2022). Short term OPA1 loss also led to a sharp increase in SCs committed to differentiation, suggesting mitochondrial organization and energy output plays a key role in SC fate decisions. Conversely, it was also found that overexpression of OPA1 in SCs promoted a deeper quiescent state due to the increased mitochondrial fusion and higher Oxphos activity (Baker et al., 2022). This deeper quiescent state is similar to the population of SCs with a higher Pax7 expression (Baker et al., 2022; Rocheteau et al., 2012).

Mitochondrial fission through Drp1 also plays an important role in SC fates. When Drp1 activity is heightened in muscle stem cells, the cells displayed fragmented mitochondria that had lower ATP production and increased oxidative stress (Jheng et al., 2012). However, Drp1 is required for the differentiation process. In early myogenic differentiation Drp1 is upregulated to cause mitochondrial fragmentation (Sin et al., 2016). Moreover, if Drp1 is not repressed before terminal differentiation then it does not occur, but complete inhibition of Drp1 causes a total loss in differentiation potential. (Kim et al., 2013; Palma et al., 2010).

1.8 The NAD^+/NADH ratio and sirtuins

The ratio of NAD^+ and NADH can be used as markers for the cellular redox state (Lunt and Heiden, 2011). The NAD^+/NADH ratio is indicative of the balance between Oxphos and glycolysis, as to re-form NAD^+, NADH is reduced by the mitochondrial ETC, while glycolysis and the TCA generates NADH (Yang and Sauve, 2016). Imbalances in this ratio can be caused by dysfunctions in the ETC. Indeed, loss of mitochondrial ETC activity (specifically complex I/III) causes a backup of electron shuttling in the ETC, which decreases the mitochondrial NADH reduction rate (Yang and Sauve, 2016). This causes the NAD^+/NADH ratio to decrease, which also lowers overall cellular Oxphos levels and results in mitochondrial fragmentation (Yang and Sauve, 2016). When glycolysis is the primary source of energy metabolism, which is typically seen in proliferating cells, the cellular NAD^+/NADH ratio is low (Lunt and Heiden, 2011). Conversely, the NAD^+/NADH ratio can be increased under certain conditions as well. Specifically, for reduced glucose levels, glycolysis is limited, forcing cells towards Oxphos for energy production, resulting in mitochondrial fusion (Song and Hwang, 2019; Rossignol et al., 2004). The shift in NAD^+/NADH ratio affects many cellular processes related to metabolism, but most notably

affects the sirtuin class of deacetylases. The sirtuins belong to the class III histone deacetylases but are unique in that their activity is tied to the availability of NAD^+. Thus, they are susceptible to modulation by the cellular NAD^+/NADH ratio and can deacetylate proteins other than histones (Grabowska et al., 2017; Kupis et al., 2016; Xie et al., 2020). NAD^+ is a reactant for their deacetylase activity, forming 2′-O-acetyl-ADP-ribose while deacetylating a target substrate (Grabowska et al., 2017).

Seven sirtuins (Sirt1-7) are found in mammals, each possessing a unique function or localization (Kupis et al., 2016). Sirt1-2 are localized in the nucleus and cytoplasm, Sirt3-4 exclusively in the mitochondria, Sirt5 is present in all compartments, and Sirt6-7 are exclusively found in the nucleus (Kupis et al., 2016). Though the sirtuins all serve critical functions, Sirt1, Sirt2 and Sirt3 have a role in muscle.

Sirt1 has been well documented for its function in SC differentiation, as its attenuation is necessary for terminal differentiation of myofibers (Fulco et al., 2003, 2008; Ryall et al., 2015). Its function is linked with epigenetic regulation of the myogenic program, as its histone deacetylase activity suppresses genes involved with differentiation by preventing their acetylation and subsequent expression (Ryall et al., 2015). During muscle differentiation, Sirt1 expression and the NAD^+/NADH ratio was found to decrease throughout the process, and cells overexpressing Sirt1 failed to fully differentiate (Fulco et al., 2003).

Other studies found that Sirt1 activity was necessary for proper SC functioning Myers et al. found that loss of Sirt1 in SCs hindered proliferation in response to injury, while loss of Sirt1 in muscle tissue had little to no effect (Myers et al., 2019). Notably, it was also found that Sirt1 activity is responsible for the transition from quiescence to activation (Tang and Rando 2014). While Ryall et al. had found that Sirt1 was responsible for maintaining quiescence and delaying

activation, Tang and Rando found that Sirt1 activity promoted the transition to activation in SCs, and its deletion delayed activation (Ryall et al., 2015; Tang and Rando, 2014). In this case, Sirt1 was acting to promote autophagic flux, which was hypothesized to be necessary for the cell to produce enough metabolites for activation and proliferation (Tang and Rando, 2014). These contradictory results suggest a more complicated, multifaceted role for Sirt1 in maintenance of SC quiescence and activation, and proliferation that might be related to differences in the knockout model, mouse strain and criteria used to discriminate the various phases between the studies.

Sirt2 has recently been demonstrated to target Pax7, and influence SC fate decisions (Sincennes et al., 2021). It was found that Pax7 contains two acetylation sites at K^{105} and K^{193}, and acetylation of these sites causes attenuation in Pax7 activity (Sincennes et al., 2021). When deacetylated, Pax7 causes an increase in self-renewal at the expense of commitment to differentiation (Sincennes et al., 2021). Additionally, the change in self-renewal causes a decrease in asymmetric divisions, increasing the number of Myf5- cells through symmetric divisions. Conversely, the opposite effect is shown upon Sirt2 inhibition. Pax7 remains acetylated, and the expression of Myf5 is dramatically increased (Sincennes et al., 2021). Thus, Sirt2 is directly responsible for the deacetylation of Pax7, which can influence fate decisions and division types.

Sirt3 is localized exclusively to mitochondria where it regulates the acetylation status of mitochondrial proteins. Sirt3 serves a vital role, as deacetylation of mitochondrial proteins serves to regulate their activity (Kupis et al., 2016). This function of Sirt3 was highlighted in a study done by Lee et al., who found that when the cellular NAD^+/NADH ratio is low, Sirt3 activity is attenuated, leading to hyperacetylation of mitochondrial proteins and mitochondrial dysfunction (Lee et al., 2016). Highlighting the role metabolism has in regulation of protein acetylation, Karamanlidis et al., found that a reduction in ETC complex I led to the reduction in the cellular

NAD^+/NADH ratio, sufficient to inhibit Sirt3 activity, which resulted in the hyperacetylation of mitochondrial proteins (Karamanlidis et al., 2013). Sirt3 genetically deleted mice, also resulted in hyperacetylation and lack of activity of mitochondrial proteins (Karamanlidid et al., 2013). This hyperacetylation effect upon Sirt3 deletion was also found in OPA1 (Samant et al., 2014). As Sirt3 is dependent on the mitochondrial NAD^+/NADH ratio, OPA1 activity is thereby indirectly tied to the cellular redox state (Karamanlidis et al., 2013). To date there is no data available for the role of Sirt3 in SCs.

1.9 p107 and SC metabolism

Retinoblastoma like protein 1 (Rbl1, p107) is a part of the retinoblastoma family of transcriptional co-repressors, which include retinoblastoma protein (Rb1, Rb) and retinoblastoma like protein 2 (Rbl2, p130). p107, as with its family members, can influence cell cycle progression (Henley and Dick, 2012). Knockdown of p107 has been shown to increase transcription of G1/S phase and G2/M phase genes, while overexpression of p107 delays or blocks entry into the S phase of the cell cycle (Schade et al., 2019; Rodier et al., 2005). p107 functions by preferentially binding to and modulating the activity of the E2F4 transcription factor, exerting its suppressive effect when bound (Xiao et al., 1996; Wirt and Sage, 2010). This interaction is interrupted by the phosphorylation of p107 by cyclin dependent kinases, which dissociate p107 from E2F4, relieving its suppression of target genes (Zhu et al., 1995). A unique feature of p107 is that its expression is limited to only proliferating cells, as it is not expressed during quiescence or in terminally differentiated cells (Henley and Dick, 2012; Wirt and Sage, 2010).

The Rb protein family also has a non-canonical role with their ability to influence the energy status of cells (Fajas, 2013). p107 has been shown to affect the fate of adipocyte progenitors

(Porras et al., 2017; De Sousa et al., 2014; Scimè et al., 2005). When adipose tissue from p107 genetically deleted (p107KO) mice was analyzed, it was shown to develop the oxidative thermogenic brown and beige adipocytes, rather than white (De Sousa et al., 2014; Scimè et al., 2005). Adipogenic progenitors from the stromal vascular fraction of p107KO adipose tissue and p107KO murine embryonic fibroblasts (MEFs) differentiated preferentially into oxidative thermogenic type adipocytes (De Sousa et al., 2014). Moreover, p107 exerts its effects on adipocyte lineage fates through its control over the cellular metabolic profile. p107 depleted growth arrested adipogenic progenitors displayed an aerobic glycolytic profile where despite the presence of oxygen, pyruvate was converted to lactate, rather than being shuttled to the TCA cycle. This was required to drive commitment to the thermogenic adipocyte lineage (Porras et al., 2017). These studies highlight a function that p107 has in controlling progenitor fate decisions through its influence of metabolism.

In skeletal muscle, p107 has been shown to influence muscle fiber type composition. p107KO mice displayed higher levels of the oxidative type I and IIA muscle fibers in mice of the Balb/c strain (Scimè et al., 2010). Indeed, primary muscle progenitors (MPCs) of p107KO mice differentiated into more highly oxidative myotubes compared to controls (Scimè et al., 2010).

Recently, our lab discovered that p107 has a mitochondrial role in reducing Oxphos capacity in the C2C12 MPC line (Bhattacharya et al., 2021). It was determined that p107 interacted at the mtDNA to repress transcription of mitochondrial genes, and reduce Oxphos capacity (Bhattacharya et al., 2021). Conversely, p107KO C2C12 cells displayed higher levels of Oxphos, a more interconnected mitochondrial network, and enhanced mitochondrial gene expression compared to controls (Bhattacharya et al., 2021). Additionally, it was found that the mitochondrial function of p107 acted in a Sirt1 dependent manner, with its mitochondrial localization inhibited

by Sirt1 activation. This was confirmed through analysis of the NAD^+/NADH ratio, which found that when the ratio was high and Sirt1 was active, p107 was sequestered in the cytoplasm, and when low, lack of Sirt1 activity allowed for p107 to enter the mitochondria (Bhattacharya et al., 2021). Moreover, it was found that p107 and Sirt1 directly interacted with each other, demonstrating that p107 is a binding partner for Sirt1 (Bhattacharya et al., 2021). A notable feature of p107KO C2C12 cells is the presence of a hyperfused mitochondrial network, compared to controls. This increase in mitochondrial fusion is associated with an increase in mitochondrial respiration, with p107KO C2C12 cells displaying a higher oxygen consumption rate than their wildtype counterparts (Bhattacharya et al., 2022). Thus, not only does a lack of p107 increase mitochondrial fusion, but it also results in a functional increase in mitochondrial Oxphos, highlighting a non-canonical non-nuclear function.

CHAPTER 2

RATIONALE, HYPOTHESIS, AND OBJECTIVES

Rationale

Though p107 has been demonstrated to influence the metabolism and fate decisions of adipogenic progenitors, this control has yet to be fully elucidated in muscle SCs (De Sousa et al., 2014; Porras et al., 2017; Scimè et al., 2005). Also, our lab has published a non-canonical non-nuclear mitochondrial role for p107 in the control of muscle progenitor cell metabolism (Bhattacharya et al., 2021). Further, unpublished work from our lab shows that SCs isolated from p107KO mice display a preference for self-renewal upon activation, without attenuating differentiation and regenerative capacity (Shah, 2023). Upon further investigation, it was found that this effect was attributed to the lack of p107 localized to the mitochondria. However, the exact mechanism in which p107 exerts its control over fate decision making remains unknown. This investigation into the role and mechanism of mitochondrial p107 in SCs may provide novel insight into the pathways that affect SC fate decisions.

Hypothesis

We hypothesize that p107 mitochondrial localization regulates mitochondrial dynamics to influence SC fate decisions.

Objectives

The primary objective of this research project is to determine if mitochondrial p107 influences SC fate decisions by three specific objectives.

Aim 1: To determine if p107 is regulated by the NAD/NADH ratio and sirtuin activity in SCs.

Aim 2: To determine how p107 mitochondrial localization affects SC fate decisions.

Aim 3: To assess the potential role of p107 in SC mitochondrial dynamics.

CHAPTER 3

MATERIALS AND METHODS

Mice

Animal experiments were performed according to guidelines approved by the York University Animal Care Committee, based on the guidelines of the Canadian Council on Animal Care. Wild type (WT) and p107 genetically deleted (p107KO) mice (LeCouter et al., 1998) used in animal experiments and tissue extraction were of mixed strain (NMRI, C57/Bl6, FVB/N) background (Chen et al., 2004). All mice used were 6 to 8 weeks of age, with male and female mice being used indiscriminately.

Cell culture

The C2C12 myogenic progenitor cell line was purchased from the American Tissue Type Culture. Cells were grown in 25mM glucose Dulbecco's Modified Eagle Medium (DMEM) (Wisent Bioproducts) supplemented with 10% fetal bovine serum (FBS) (Wisent Bioproducts), and 1% penicillin streptomycin (P/S) (Wisent Bioproducts) and incubated at 37°C with 5% CO_2.

Glucose availability experiments

For in vitro cell culture experiments comparing effects of glucose availability, stripped DMEM lacking glucose, sodium pyruvate, HEPES, L-glutamine, and phenol red (Gibco, ThermoFisher) supplemented with 10% FBS and 1% P/S was used. For primary myofiber culture, stripped DMEM was supplemented instead with 20% FBS, 1% P/S, 1% chicken embryo extract (CEE) (MP Biomedicals), and 7.5ng/mL basic fibroblast growth factor (bFGF) (PeproTech). To

achieve desired glucose concentrations, D-glucose (Sigma Aldrich) was added to attain 25mM and 5.5mM glucose concentrations.

For nicotinamide (NAM) experiments, 10mM of nicotinamide (Alfa Aesar) was added to the 5.5mM glucose stripped DMEM fiber culture medium. NAM supplemented medium was added to culture 24h post-isolation, to avoid interference of SC activation.

Primary myofiber isolation

Extensor digitorum longus (EDL) myofibers were isolated from WT and p107KO mice. Mice were sacrificed and EDL muscles were dissected with tendons intact and digested in filter sterilized 0.2% type 1 collagenase (Sigma Aldrich) in FBS free DMEM for 45 minutes in a 37°C water bath. Once the EDL was sufficiently digested, muscles were transferred to warmed cell culture dishes containing DMEM and 1% P/S. Muscles were then flushed with a Pasteur pipette to release the individual myofibers. Myofibers were then picked up using a Pasteur pipette and transferred to a 12 or 24 well plate containing warm 25mM glucose DMEM supplemented with 20% FBS, 1% P/S, 1% CEE, and 7.5ng/mL bFGF and cultured at 37°C with 5% CO_2 for 72 hours.

A minimum of 15 myofibers from each unique condition were analyzed for all myofiber experiments. Activated, self-renewing, and differentiating SCs were counted and expressed as a fraction of the total SC population in the group. Data was expressed as a fold change of the fraction of activated, self-renewing, or committed SCs compared to the total SC population.

Western blot analysis

Cells were lysed in RIPA buffer (0.5% NP-40, 0.1% sodium deoxycholate, 150mM NaCl,

50mM Tris-Cl pH 7.5, 5mM EDTA), supplemented with a protein inhibitor cocktail containing 1mg/mL pepstatin, aprotinin, and leupeptin. The mixture was incubated on ice for 10 minutes before being centrifuged at 21000g for 15 minutes at 4°C to remove cellular debris.

Protein lysates were boiled in a buffer containing 4% SDS, 10% 2-mercaptoethanol, 20% glycerol, 0.004% bromophenol blue, 0.125M Tris HCl and 1mM DTT for 3 minutes. After loading onto either gradient (6-12%) or 8% sodium dodecyl sulfate–polyacrylamide gel electrophoresis (SDS-PAGE) gels, samples were run in buffer composed of 25mM Tris base, 192mM glycine and 0.1% SDS and proteins were separated by electrophoresis for approximately 1 hour and 30 minutes at 30 milliamps. Proteins from the gel were transferred onto 0.22μM pore size nitrocellulose membrane (Santa Cruz Biotechnology) in a buffer containing 50mM Tris base, 384mM glycine, and 20% methanol for 1 hour and 20 minutes. Membranes were then blocked for 1 hour at room temperature in 5% non-fat milk in Tris-buffered saline (TBS) (50mM Tris-base and 150mM NaCl) with 0.1% Triton X-100 (TBST) and then washed for 3 minutes in TBST. The membranes were probed overnight at 4°C with primary antibodies diluted in 1% bovine serum albumin (BSA) in TBST with gentle rocking. The next day, membranes were washed with TBST and incubated for 1 hour at room temperature with secondary antibodies, either goat anti-rabbit or goat anti-mouse (Bio-Rad) conjugated with horseradish peroxidase, diluted in 5% non-fat milk in TBST with gentle rocking. After secondary antibody incubation, membranes were washed in TBST 3 times for 5 minutes and finally washed in TBS for 10 minutes. Membrane visualization was done using chemiluminescence Clarity Western ECL Substrate (Bio-Rad) on photographic UltraCruz Autoradiography Film (Santa Cruz Biotechnology). Protein levels were evaluated through densitometry using Image J software. The densitometric values were presented as fold changes of the ratio of the protein of interest compared to the loading control α-tubulin. For **Fig. 4.14B**,

densitometric values were taken from the red hashed box from **Fig. 4.14A**. All Western blotting consisted of at least three clonal cell lines.

Real-time quantitative polymerase (RT-qPCR)

For RNA isolation, cells were lysed using QIAzol Lysis Reagent (Qiagen). Lysed samples were incubated at room temperature for 5 minutes, and 200µL of chloroform (Sigma Aldrich) was added per milliliter of QIAzol used. Samples were mixed and incubated at room temperature for 5 minutes before centrifugation at 12000g for 15 minutes at 4°C. The uppermost phase was retained, with the other layers being discarded. For each milliliter of QIAzol used, 500µL of isopropyl alcohol (Sigma Aldrich) was added to the retained phase and incubated at room temperature for 10 minutes. Samples were then centrifuged at 12000g for 10 minutes at 4°C. The supernatant was discarded, and the pellet retained. The pellet was washed twice by adding 1mL of 75% ethanol (Sigma Aldrich) per 1mL of QIAzol used, shaking, then centrifuging at 7500g for 5 minutes at 4°C. The pellet was once again retained, and the tube containing the pellet was opened and placed upside down and let to air dry for 10 minutes. RNA pellet was resuspended in RNAse free water, and its concentration was measured using the NanoDrop ND-1000 UV-Vis Spectrophotometer (ThermoFisher). To convert RNA into cDNA, the Advanced cDNA (Wisent Bioproducts) kit was used according to the manufacturer's instructions.

For RT-qPCR, samples were loaded in duplicate into a 96-well PCR plate. Each well contained 1x SYBR Green dye (BiMake), 1µM OPA1 forward primer (TGGAAAATGGTTCGAGAGTCAG), 1µM OPA1 reverse primer (CATTCCGTCTCTAGGTTAAAGCG), 25ng of cDNA template, and water to make 20µL reaction volume. Plates were briefly centrifuged at 425g for 5 minutes to ensure all reagents were

mixed at the bottom of each well. PCR was carried out on the LightCycler 96 system (Roche), with 40 amplification cycles. Results were then analyzed for changes in gene expression using the 2(-Delta Delta C(T)) method (Livak and Schmittgen, 2001). Gene expression data was presented as the fold change between the 2(-Delta Delta C(T)) values. Three clonal cell lines were used.

p107KO cell line derivation

Crispr/Cas9 was used to generate the p107 genetically deleted (p107KO) C2C12 cell lines used. C2C12 cells were transfected with 3 LentiU6-sgRNA-SFFV-Cas9-2A-Puro plasmids each containing a different sgRNA to target p107 sequences 110 CGTGAAGTCATCCAGGGCTT, 56 GGGAGAAGTTATACACTGGC, and 350 AGTTTCGTGAGCGGATAGAA (Applied Biological Materials). For transfection, 10µg of each plasmid, 2.5mM $CaCl_2$, and distilled water to 500µL was added dropwise into HEBS buffer (274mM NaCl, 10mM KCl, 1.4mM Na_2HPO_4, 15mM D-glucose and 42mM HEPES), incubated at room temperature for 1 hour, then added to 20% confluent C2C12 cells.

To select clones, 18 hours post-transfection, the cells were passaged into 96 well tissue culture plates and 2mg/mL puromycin in DMEM supplemented with 5% FBS and 1% P/S was added 24 hours after passaging that was refreshed after 2 days 3 times. Surviving clones were cultured and tested for p107 knockout through Western blotting. For control cells, C2C12 cells were transfected with an empty vector pLentiU6-sgRNA-SFFV-Cas9-2A-Puro and puromycin selected as above.

Immunocytochemistry and confocal imaging

To visualize myofiber associated SCs, WT and p107KO myofibers were fixed for 10 minutes in prewarmed 2% PFA in phosphate buffered saline (PBS) with gentle rocking at room

temperature. Myofibers were washed 3 times with PBST (0.1% Triton X-100 in PBS) and incubated with permeabilization buffer (0.3% Triton X-100 and 0.1M glycine in PBS) for 10 minutes at room temperature with gentle rocking. Myofibers were then incubated for 1 hour at room temperature with gentle rocking in blocking buffer (2% BSA, 5% donkey serum, 5% goat serum and 0.1% Triton X-100 in PBS). After blocking, myofibers were incubated in blocking buffer containing primary p107 (p107-SD9 Santa Cruz Biotechnology) or Pax7 (AB_528428 DSHB) antibody at a 1:100 dilution overnight at 4°C. The next day myofibers were washed 3 times with PBST, then incubated with anti-mouse secondary antibodies NL 493 conjugated (NL009 Novus Biologicals) or NL 557 conjugated (NL007 Novus Biologicals) at a 1:1000 dilution for 1 hour at room temperature with gentle rocking. The myofibers were then washed 3 times with PBST, before being incubated at 4°C overnight with blocking buffer containing a 1:100 dilution of primary antibody MyoD (NBP1-54153 Novus Biologicals) or Tom20 (11802-1-AP Proteintech), with gentle rocking. The next day, myofibers were once again washed 3 times with PBST, then incubated for 1 hour at room temperature with gentle rocking in blocking buffer with anti-rabbit secondary antibody NL 637 conjugated (NL005 NovusBiologicals) at a 1:1000 dilution. After incubation, myofibers were washed 3 times with PBST and incubated with 10µg/mL DAPI (Sigma Aldrich) for 10 minutes with gentle rocking at room temperature, then washed 3 times with PBST. Myofibers were then mounted onto positively charged microscope slides (FroggaBio) and Vectashield mounting media (Vector) was added before placing a coverslip and sealing the slide. Confocal imaging of individual SCs and SC clusters was done using the LSM 700 microscope with Plan-Apochromat 63x/1.4 III HR (Zeiss) optical equipment. A line was drawn through representative cells to indicate relative intensity of RGB signals for colocalization analysis with Zen Blue software (Zeiss). The values were then plotted and congruent peaks were manually

evaluated with the criteria that both intensity lines must peak at the same point on the X axis. This was repeated three times with different biological replicates for each treatment group, and the number of congruent peaks were compared as a fold change to each other across treatment groups.

Antibodies used

α-tubulin (66031-1-Ig Proteintech); Acetyl-Lysine (9441 Cell Signaling); MyoD (NBP1-54153 Novus Biologicals); Pax7 (AB_528428 DSHB); Pax7 (20570-1-AP Proteintech); p107 (13354-1-AP Proteintech); p107 (p107-SD9 Santa Cruz Biotech); Tom20 (11802-1-AP Proteintech); Goat anti-rabbit IgG (H+L) HRP Conjugate (170-6515 BioRad); Goat Anti-Mouse IgG (H+L) HRP Conjugate (170-6516 BioRad); Donkey Anti-Mouse IgG Secondary Antibody NL 493 conjugated (NL009 Novus Biologicals); Donkey Anti-Mouse IgG Secondary Antibody NL 557 conjugated (NL007 Novus Biologicals); Donkey Anti-Rabbit IgG Secondary Antibody NL 637 conjugated (NL005 NovusBiologicals).

Live cell imaging

For live cell imaging of mitochondria, control and p107KO C2C12 cells were first cultured to 50% confluency in Nunc Lab-Tek II chamber slides (ThermoFisher) before they were grown in 5.5mM or 25mM glucose stripped medium for 24h prior to imaging. 40mM MitoView Green (ThermoFisher) was added to each of the cell cultures and incubated for 10 minutes at 37°C. Cells were then live imaged with the Axio Observer.Z1 microscope with Plan-Apochromat 63x/1.4 III HR (Zeiss) optical equipment.

Mitochondrial measurements

Using confocal microscopy images, mitochondrial length was measured by tracing over the mitochondria from one end to the other with a line that was calibrated to the scale bar using Image J software. When measuring mitochondria, at least 200 mitochondria were counted in C2C12 culture models, while at least 50 mitochondria were counted for ex vivo myofiber models. For C2C12 live cell imaging, at least three clonal cell lines were used, and for SCs from myofibers, 3 independent mice were used.

Statistics and Reproducibility

All experiments were performed with at least three biological replicates, as indicated in figure legends. Results were presented as the mean ± standard deviation. Statistical analysis was performed using two tailed Student's T-tests in Microsoft Excel and were considered statistically significant when $p<0.05$. Some data were analyzed using an appropriate two-way analysis of variance (ANOVA) with the criteria of $p<0.05$. All significant differences were subsequently evaluated using a Tukey post hoc test.

CHAPTER 4

RESULTS

Localization of p107 in SCs is controlled by glucose availability

In the C2C12 MPC cell line, p107 was recently demonstrated to be localized in the mitochondria in cells grown in 25mM glucose, and conversely in the cytoplasm when grown with 5.5mM (Bhattacharya et al., 2021). As this relationship was never demonstrated in SCs, the adult muscle stem cells, we assessed p107 localization by using ex vivo myofibers isolated from mouse EDL cultured in medium containing either 25mM or 5.5mM glucose, without pyruvate and glutamine. First, we evaluated localization in SCs grown in 25 mM glucose when p107 is in the mitochondria of C2C12 cells. p107 in SCs was visualized after three days in culture by immunofluorescent staining for p107 and mitochondria marker Tom20 (mitochondrial translocase of the outer membrane complex), and subsequent confocal microscopy. Analysis of confocal Z-stack images revealed that p107 and Tom20 colocalized with many regions of immunofluorescent overlap of intense bright yellow signal (highlighted with white arrows) (**Fig. 4.1**). Colocalization was confirmed through analysis of fluorescence intensity peaks of a line scanned for the red, green, blue (RGB) profile of a representative image. Through the analysis of peak congruence between the Tom20 and p107 channels, it was observed that many intensity peaks between p107 and Tom20 were aligned, indicating large amounts of overlap, suggesting co-localization (**Fig. 4.1**).

We determined if growth in 5.5mM glucose would have the opposite effect of shifting p107 from the mitochondria of SCs to the cytoplasm, as in C2C12 cells (Bhattacharya et al., 2021). Confocal microscopy for p107 and Tom20 immunofluorescence revealed a substantial reduction of p107 located in the mitochondria compared to cells grown in 25mM glucose (**compare Fig. 4.1**

with Fig. 4.2). Staining revealed disparate areas of p107 and Tom20 staining, that was confirmed through the analysis of fluorescence intensity peaks of a line scanned for the RGB profile of the representative image (**Fig. 4.2**). The number of congruent peaks is noticeably lower than what is found in the 25mM glucose culture (**compare Fig. 4.1 with Fig. 4.2**), indicating areas without significant p107 and Tom20 overlap. Thus, these results suggest that p107 mitochondrial localization in SCs is controlled by glucose levels that regulate the NAD^+/NADH ratio (Bhattacharya et al., 2021).

Inhibition of Sirt activity results in p107 mitochondrial localization

As the NAD^+/NADH ratio is affected by glucose concentration alters p107 localization, we explored the possibility of manipulating p107 localization in SCs by influencing Sirt activity. In C2C12 cells, Sirt1 activity is known to prevent p107 mitochondrial localization whereas the Sirt inhibitor nicotinamide (NAM) has the opposite effect (Bhattacharya et al., 2021). Thus, we blocked Sirt activity in SCs using NAM to determine if it would increase p107 localization to the mitochondria. NAM was added to wildtype (WT) EDL myofiber cultures grown in 5.5mM glucose, which is a growth condition that induces significant p107 cytoplasmic localization. Confocal microscopy after immunostaining with p107 and Tom20 revealed an almost complete overlap between regions of p107 and mitochondrial marker Tom20 in SCs, suggesting that p107 localized preferentially to the mitochondria (**Fig. 4.3**). This was verified by analyzing the fluorescence intensity peaks of a line scanned for the RGB profile of the representative image (**Fig. 4.3**). A considerable number of congruent peaks are present between p107 and Tom20, indicating p107 was preferentially localized to the mitochondria.

We next evaluated the extent of p107 localization in the mitochondria by comparing the number of congruent immunofluorescent intensity peaks between p107 and mitochondria marker Tom20 that were present between SCs grown in 5.5mM glucose with and without NAM and in 25mM glucose. We find that NAM treatment and SCs grown in 25mM glucose have similar number of congruence peaks that are significantly different than SCs grown in 5.5mM glucose (**Fig. 4.4**). This indicates that Sirt inhibition appears to increase the number of p107 proteins localized in the mitochondria when the SCs are grown in 5.5mM glucose to levels of SCs grown in 25mM glucose. Our results therefore suggest that p107 mitochondrial function is controlled by Sirt activity and potentially Sirt1 as in C2C12 cells.

Mitochondrial p107 favors SC fate decisions for commitment to differentiation over self-renewal

We next determined if the mitochondrial function of p107 affects SC fate decisions. Previous unpublished data from our lab showed that p107KO SCs and p107 cytoplasmic localization in WT SCs showed a preference for self-renewal (Shah, 2023). This suggests that mitochondrial localized p107 would have the opposite effect to promote commitment to differentiate over self-renewal. To test this possibility, we sought to localize p107 into the mitochondria by influencing Sirt activity and analyze SC fate decisions. SCs preferentially self-renew when grown in 5.5mM glucose conditions (Shah, 2023), which is when p107 is preferentially in the cytoplasm (**Fig. 4.2**). Thus, we treated SCs with 5.5mM glucose supplemented with NAM to localize p107 to the mitochondria (**Fig. 4.3**), in this way we can determine if SC fates change due to glucose availability or to p107 mitochondrial function.

SC fate decisions on myofibers can be observed through microscopy after immunostaining for the markers Pax7 and MyoD from two days post isolation (Brun et al., 2018). Self-renewing SCs are classified by the exclusive presence of Pax7 (Pax7+/MyoD-), activated or proliferating SCs express both Pax7 and MyoD (Pax7+/MyoD+), whereas SCs committed to differentiation solely express MyoD (Pax7-/MyoD+). Using this approach (**Fig. 4.5A**), we found that there were no differences in activated/proliferating SCs between untreated and NAM treated SCs (**Fig. 4.5B**). However, we found significantly less self-renewal in NAM treated SCs compared to untreated controls (**Fig. 4.5B**). This occurred despite the SCs growth in 5.5mM glucose, which normally stimulates preference for self-renewal (Shah, 2023). The analysis of SCs committed to differentiation showed that their numbers increased significantly to nearly seven times that of controls (**Fig. 4.5B**). This data highlights that the mitochondrial function of p107 might affect fate decisions by promoting SCs to differentiation rather than self-renewal. It also demonstrates that p107 regulation of SC fate choices might be dependent on Sirt activity.

p107 regulates SC fate decisions through Sirt activity

As Sirt inhibition led to a decrease of SC self-renewal and a concomitant increase in commitment to differentiate, we next assessed if this was dependent on p107. For this, SCs on myofibers from p107KO mice were grown in 5.5mM glucose with and without NAM. Under this condition, if Sirt activity for SC fate choices was dependent on p107 then there should be no changes to the self-renewal phenotype. SC fate choices revealed by immunofluorescence for Pax7 and MyoD with confocal microscopy show no significant difference for proliferation/activation, self-renewal, and commitment to differentiate with the addition of Sirt inhibitor NAM (**Fig. 4.6A**

and Fig. 4.6B) Together, this data suggests that Sirt activity for regulation of SC fate choices is dependent on p107.

p107 subcellular localization affects SC mitochondrial remodeling

As mitochondrial dynamics can regulate stem cell fate decisions (Baker et al., 2022; Bhattacharya and Scimè, 2020). We next determined if p107 might influence the mitochondrial network. Thus, we explored the mitochondrial interconnectivity when p107 was localized to either the mitochondria or cytoplasm. This was first assessed in vitro, using the C2C12 cells that were cultured in either 25mM or 5.5mM glucose without pyruvate and glutamine. We measured mitochondria length by visualizing mitochondria with MitoView Green (Biotium), which incorporates into the mitochondrial membrane of live cells so that they could be imaged using live cell confocal microscopy (Bhattacharya et al., 2021). Comparing 25mM to 5.5mM glucose conditions we found stark differences in mitochondrial morphology (**Fig. 4.7A**). Under the 25mM glucose condition, mitochondria are heavily fragmented, whereas those grown in 5.5mM displayed longer branching mitochondria. By measuring the length of individual mitochondria using Image J software, we found that SCs treated with 5.5mM glucose display a significantly higher average length compared to mitochondria grown in 25mM glucose (**Fig. 4.7B**). When the mitochondrial lengths were grouped according to size, we found a larger proportion of smaller mitochondria in cells grown in 25mM glucose, while those grown in 5.5mM had primarily elongated mitochondria (**Fig. 4.7C**). Thus, this suggests that p107 mitochondrial localization influenced by NAD^+/NADH might also influence mitochondrial networking of SCs.

We next determined if p107 mitochondrial function is potentially affecting mitochondrial networking of SCs. Murine EDL myofibers were extracted and cultured for 24 hours in 25mM

glucose fully supplemented medium, then switched to either 25mM or 5.5mM glucose in medium lacking pyruvate and glutamine for 48h. SCs present on fibers were immunostained for Pax7 and Tom20 and immunofluorescence visualized by confocal microscopy. In 25mM glucose, SCs display significantly fragmented mitochondria compared to 5.5mM glucose (**Fig. 4.8A**). Evaluation of the average mitochondrial length between the two groups reveal that SCs grown in 5.5mM glucose have a significantly longer (almost double) average mitochondria length compared to growth with 25mM glucose (**Fig. 4.8B**). Grouping mitochondrial lengths by size revealed that majority of mitochondria in 25mM SCs were smaller, while the mitochondria of 5.5mM SCs had significantly greater lengths (**Fig. 4.8C**). Thus, by altering the NAD^+/NADH ratio with varying glucose concentrations, p107 localization might affect mitochondrial size and remodeling of SCs.

Glucose availability that affects mitochondrial dynamics in SCs is dependent on p107

To test if the NAD^+/NADH ratio controlled by varying the glucose concentration, might affect mitochondrial remodeling of SCs through a p107 dependent function, we evaluated p107KO C2C12 cells and SCs grown in 5.5mM or 25mM glucose. First, MitoView was added to p107KO C2C12 cells for imaging mitochondria by live cell confocal microscopy. Upon comparison between the two growth conditions, we found that p107KO C2C12 cells did not display any noticeable change in their mitochondrial length (**Fig. 4.9A**). This was confirmed through measurement of mitochondrial lengths, that showed that the average length did not change between the two groups (**Fig. 4.9B**). Furthermore, grouping according to length showed that the number of mitochondria for each of the grouped lengths varied little between the two glucose conditions (**Fig. 4.9C**). Thus, glucose conditions that vary the NAD^+/NADH ratio show no change in mitochondrial

morphology of p107KO C2C12 cells suggesting that mitochondrial network changes occur through a p107 dependent mechanism.

We then assessed SCs from p107KO mice for mitochondria networking when grown with 5.5mM or 25mM glucose as was done for p107KO C2C12 cells (**Fig. 4.9**). Analysis used Pax7 and Tom20 immunofluorescence to identify SC mitochondria that showed no immediate mitochondria morphological differences between the SCs grown in 5.5mM and 25mM glucose, as they both appeared to be highly interconnected (**Fig. 4.10A**). Evaluation of average mitochondrial length with Image J, revealed that p107KO SCs did not display any significant change in length (**Fig. 4.10B**). Also, grouping according to length size showed that the number of mitochondria of each grouped length did not significantly vary between the two glucose conditions (**Fig. 4.10C**). As varying the glucose concentration, which alters the NAD^+/NADH ratio, had no effect on p107KO SCs, it suggests that regulation of mitochondria organization by NAD^+/NADH is dependent on p107 and might be based on Sirt activity.

Sirt mitochondrial organization of SCs is dependent on p107

We explored if p107 regulation of mitochondria network organization in SCs is potentially based on Sirt activity. We assessed if Sirt activity was affecting mitochondrial network organization by growing extracted EDL myofibers containing SCs with 5.5mM glucose with and without Sirt inhibitor NAM (**Fig. 4.11**). The SCs present on the myofibers were immunostained with Tom20 and Pax7. Subsequent confocal microscopy Z-stacks of SCs showed that the mitochondria in NAM treated SCs display less definition, appearing in clumps rather than outlined in more defined structures as in the untreated control (**Fig. 4.11A**). The middle slice of the Z-stack was used for mitochondria length measurement using Image J software. Analysis of the average

mitochondrial length revealed that the NAM treated SCs displayed significantly lower average mitochondrial length than untreated (**Fig. 4.11B**). Analysis of mitochondrial length distribution shows that the non-NAM treated SCs displayed a higher number of longer mitochondria, whereas NAM treatment increased the number of shorter mitochondria (**Fig. 4.11C**).

Next, we tested if the effect of inhibiting Sirt on mitochondrial network organization was dependent on p107. For this, p107KO SCs were grown in 5.5mM glucose in the presence or absence of NAM. Confocal microscopy and immunofluorescence for Pax7 and TOM20 showed no differences in mitochondrial morphology (**Fig. 4.12A**). Analysis of average mitochondrial length between the NAM treated and non-NAM treated p107KO SCs revealed that there was no statistically significant difference in size (**Fig. 4.12B**). Also, there were no differences observed when grouping mitochondria by their size, with each treatment displaying a similar number of mitochondria of each size (**Fig. 4.12C**). Together, these results suggest that Sirt activity, potentially Sirt1, which is responsible for the change in mitochondrial morphology, is dependent on p107.

p107KO C2C12 cells express elevated OPA1 protein levels

To explore a possible mechanism for the increased mitochondrial fusion in p107KO cells compared to WT controls, we gauged the protein expression levels of mitochondrial fusion protein OPA1. Protein lysate was collected from control and p107KO C2C12 cells, and Western blotted for OPA1 (**Fig. 4.13A**). Densitometric analysis of the Western blot showed that OPA1 protein levels were significantly higher in p107KO cells compared to controls (**Fig. 4.13A**). We evaluated if the elevated OPA1 protein levels in p107KO cells was related to an increase in OPA1 gene expression. Real-time quantitative PCR (RT-qPCR) analysis of OPA1 in control and p107KO

C2C12 cells showed no differences in gene expression (**Fig. 4.13B**). This suggests a possible explanation for the increased mitochondrial fusion in the absence of mitochondrial p107 is potentially due to increased OPA1 protein levels.

p107 levels are associated with global cellular protein acetylation

As increases in OPA1 activity is due to its deacetylation, which is linked with lower global cellular acetylation levels (Parodi-Rullán et al., 2018), we assessed if p107 is associated with this process. For this, protein lysates from control and p107KO C2C12 cells were Western blotted for general global lysine acetylation. Our results showed an overall acetylation pattern of heavier (>75kda) proteins, and a general trend of higher levels of cellular acetylation in control compared to p107KO cells (**Fig. 4.14A**). This was confirmed with densitometric analysis of the darkest, bottom most bands (shown between hatched lines) that demonstrated p107KO cells with significantly lower levels of global cellular acetylation compared to controls (**Fig. 4.14B**). These results demonstrate the potential that p107 mitochondrial function might influence cellular acetylation status that impacts OPA1 activity and mitochondrial dynamics.

Figure 4.1

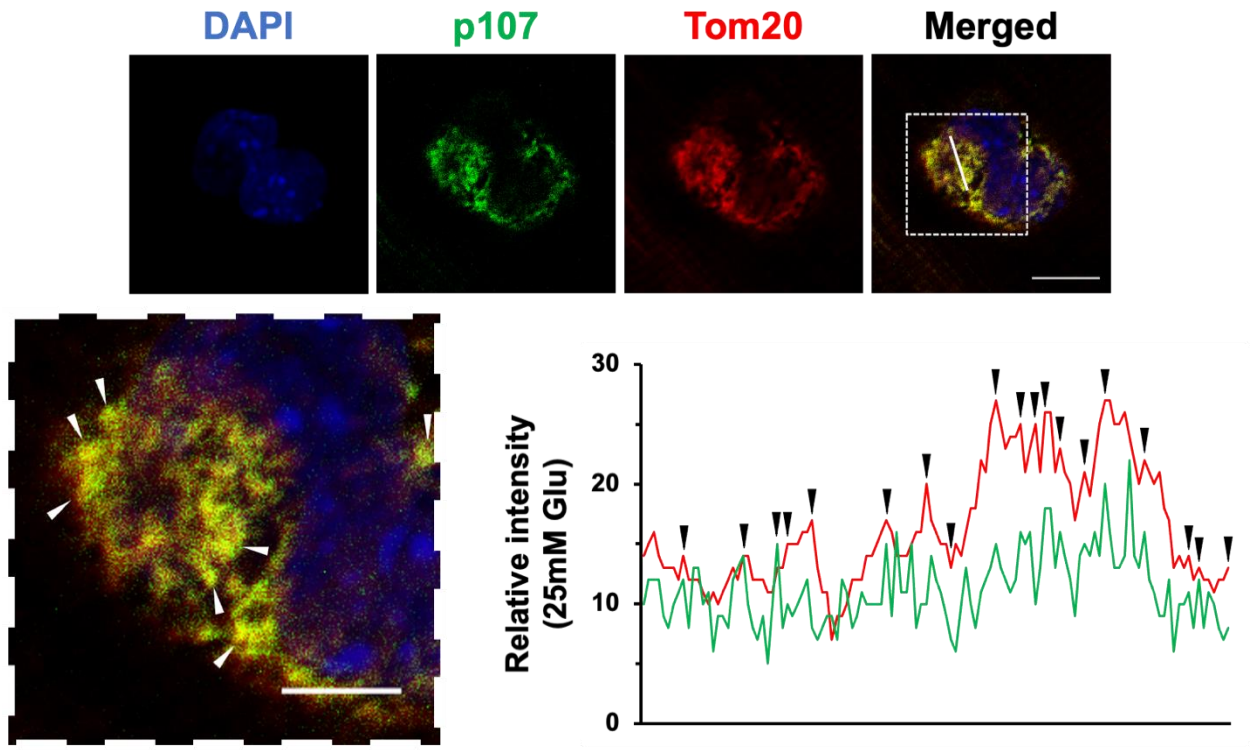

Figure 4.1. p107 is mitochondrially localized in SCs when cultured in 25mM glucose. Representative confocal microscopy images for DAPI, p107, Tom20 and merge for SCs on EDL myofiber cultured in 25mM glucose. Hashed box on merge represents a magnified image region. White arrowheads point to areas of p107 and Tom20 overlap. A line was drawn through a representative cell from the merged confocal image to indicate relative intensity of RGB signals. The black arrowheads point to areas of concurrent intensities in the images. Scale bar is 10µm, and 5µmin the magnified image.

Figure 4.2

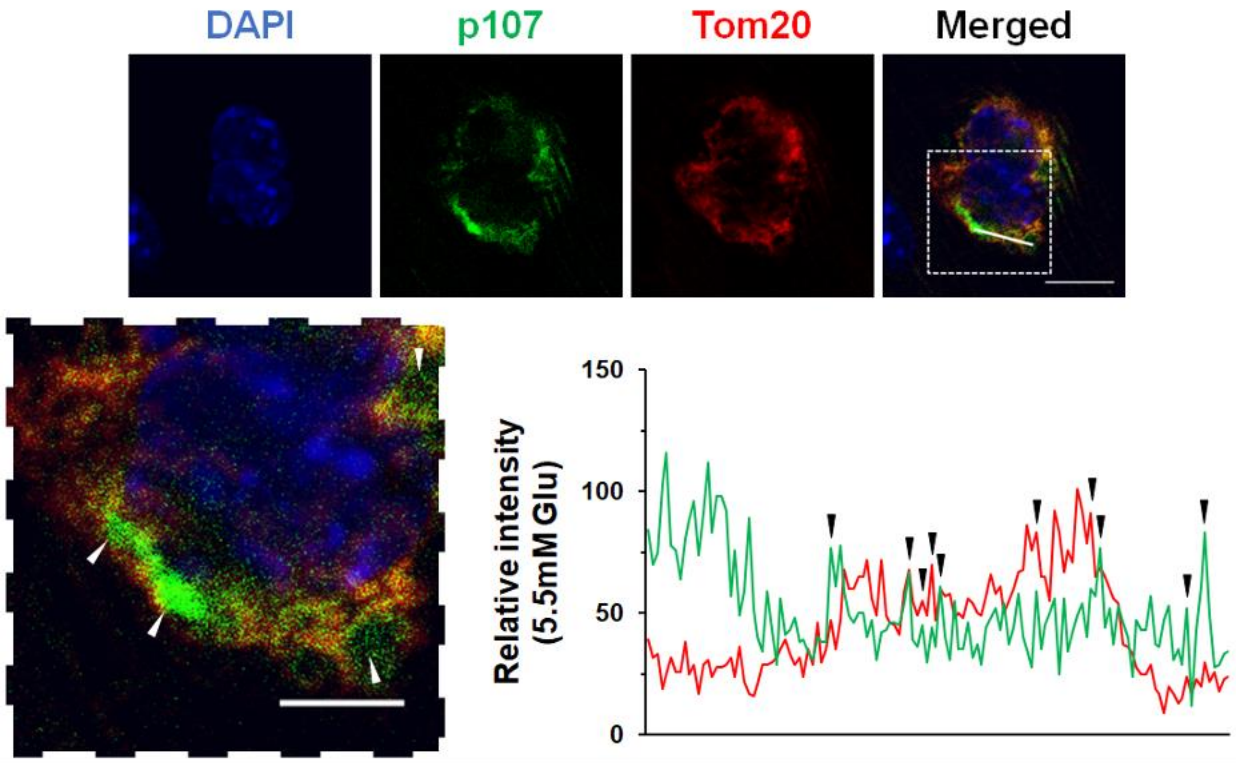

Figure 4.2. Reduced p107 mitochondrial localization in SCs cultured in 5.5mM glucose. Representative confocal microscopy images for DAPI, p107, Tom20 and merge for SCs on EDL myofiber cultured in 5.5mM glucose medium. Hashed box on merge represents a magnified image region. White arrowheads point towards areas of p107 without Tom20 overlap A line was drawn through a representative cell from the merged confocal image to indicate relative intensity of RGB signals. The black arrowheads point to areas of concurrent intensities in the images. Scale bar = 10μm, and 5μm in the magnified image.

Figure 4.3

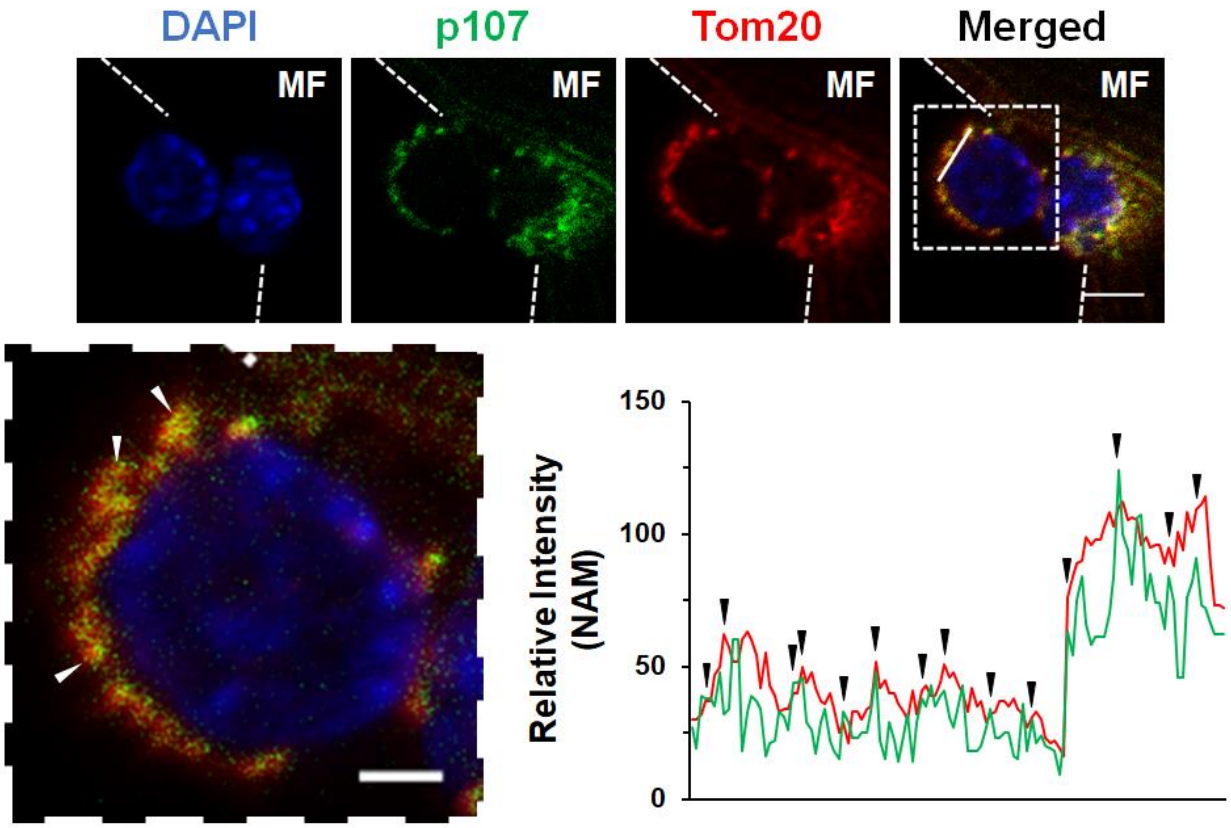

Figure 4.3. p107 preferentially localizes to the mitochondria in SCs grown with 5.5mM glucose and treated with Sirt inhibitor NAM. Representative confocal microscopy images for DAPI, p107, Tom20 and merge for SC on EDL myofiber cultured in 5.5mM glucose medium treated with NAM. Hashed box on merge represents magnified image region. White arrowheads point towards areas of p107 with strong Tom20 overlap. A line was drawn through a representative cell from the merged confocal image to indicate relative intensity of RGB signals. The black arrowheads point to areas of concurrent intensities in the images. MF denotes the area occupied by the myofiber. Scale bar = 5μm, and 2μm in the magnified image.

Figure 4.4

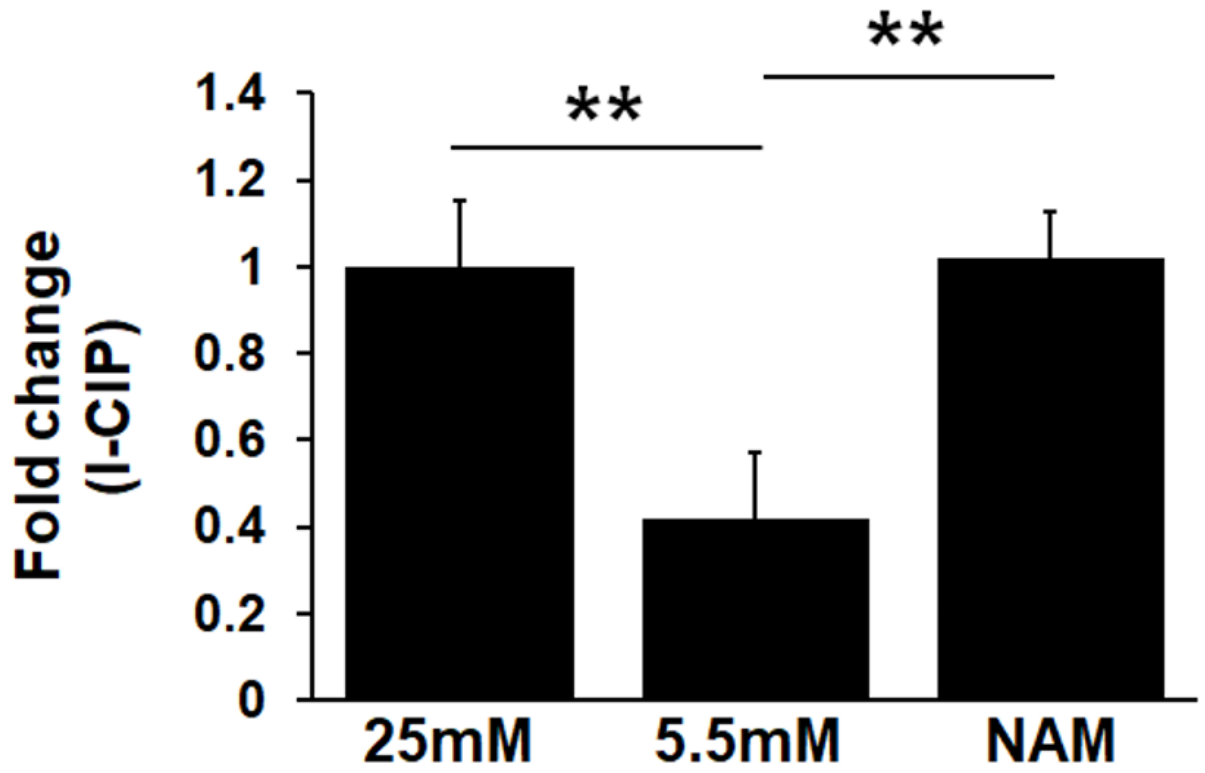

Figure 4.4. NAM inhibition of Sirt activity increases p107 and mitochondria immunofluorescent intensity overlap. Graphical representation of the fold change in the number of immunofluorescent congruent intensity peaks (I-CIP) for p107 and Tom20 of SCs on EDL myofibers grown with 25mM or 5.5mM glucose with and without NAM. n=3 mice. One way ANOVA and Tukey post hoc test was performed. $^{**}p < 0.01$.

Figure 4.5

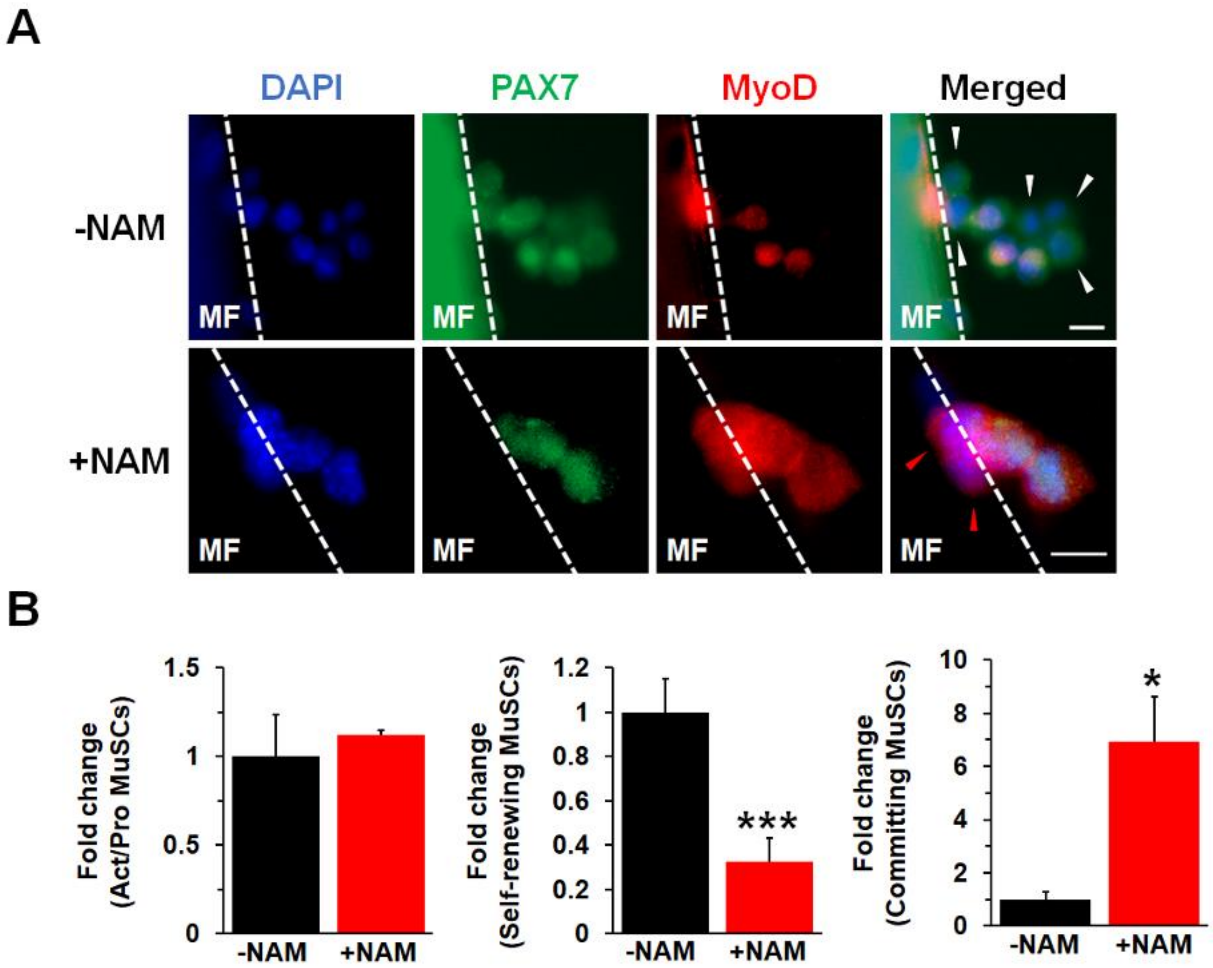

Figure 4.5. Mitochondrial localization of p107 reduces the self-renewal capacity of SCs. (A) Representative immunohistochemistry for DAPI, Pax7, MyoD and merge of SCs on EDL myofibers grown in 5.5mM glucose with or without NAM. Scale bar = 10µm. MF denotes the area occupied by the myofiber. **(B)** Graphical representation of fold change for activated or proliferating (Act/Pro), self-renewing, and committing to differentiate SCs with or without NAM. White arrows denote self-renewing SCs and red arrows denote committed SCs. Hashed lines are an outline of myofiber. Data is presented as mean values ± standard deviation. n = 4 mice. Two-tailed unpaired Student T-test, *p<0.05, ***p <0.001.

Figure 4.6

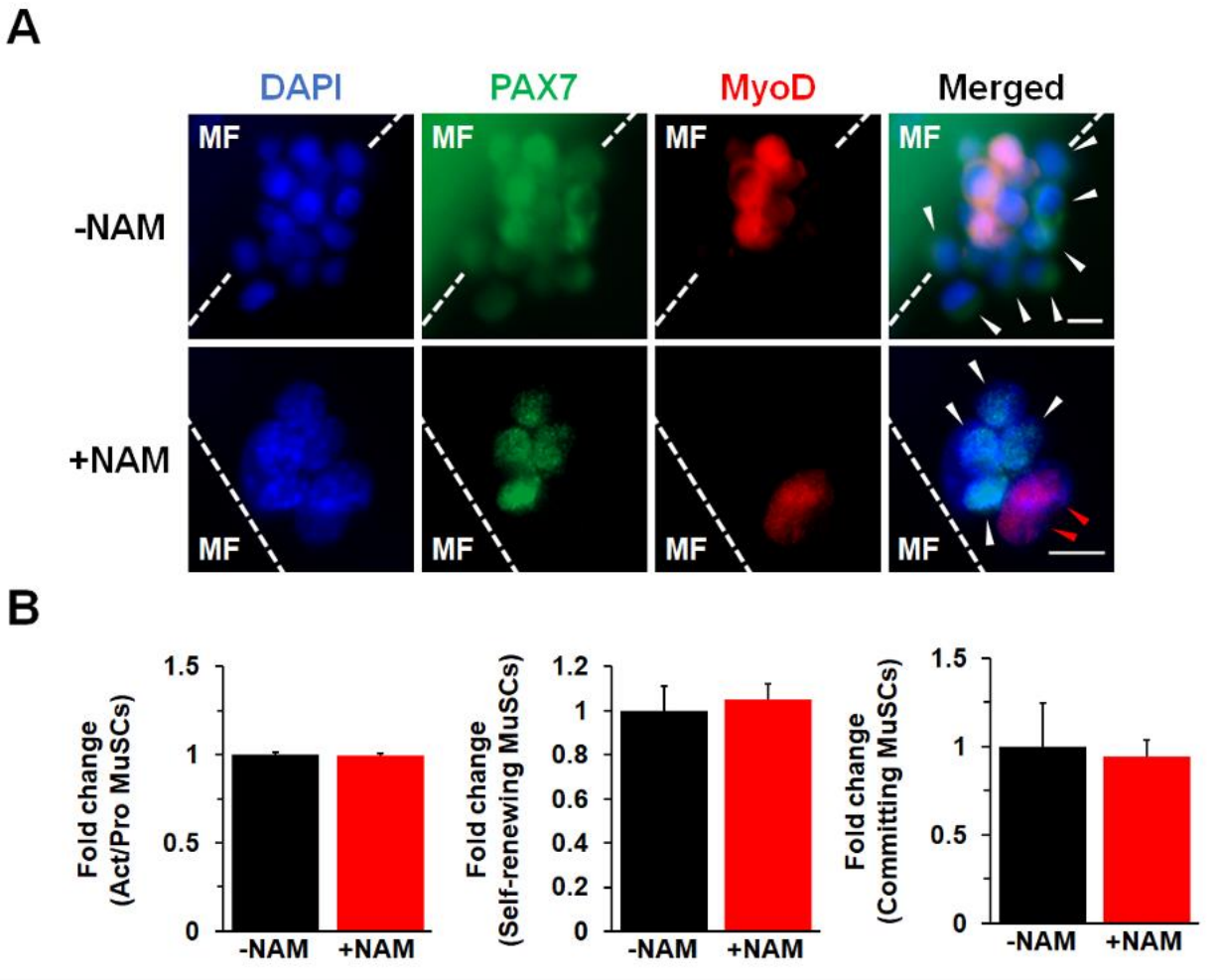

Figure 4.6. Sirt inhibition does not affect p107KO SC fate choices. (A) Representative immunohistochemistry for DAPI, Pax7, MyoD and merge of p107KO SCs on EDL myofibers grown in 5.5mM glucose with or without NAM. Scale bar = 10µm. MF denotes the area occupied by the myofiber. **(B)** Graphical representation of fold change for activated or proliferating (Act/Pro), self-renewing, and committing to differentiate SCs with or without NAM. White arrows denote self-renewing SCs, and red arrows denote committed SCs. Hashed lines are an outline of myofiber. Data is presented as mean values ± standard deviation. n = 4 mice.

Figure 4.7

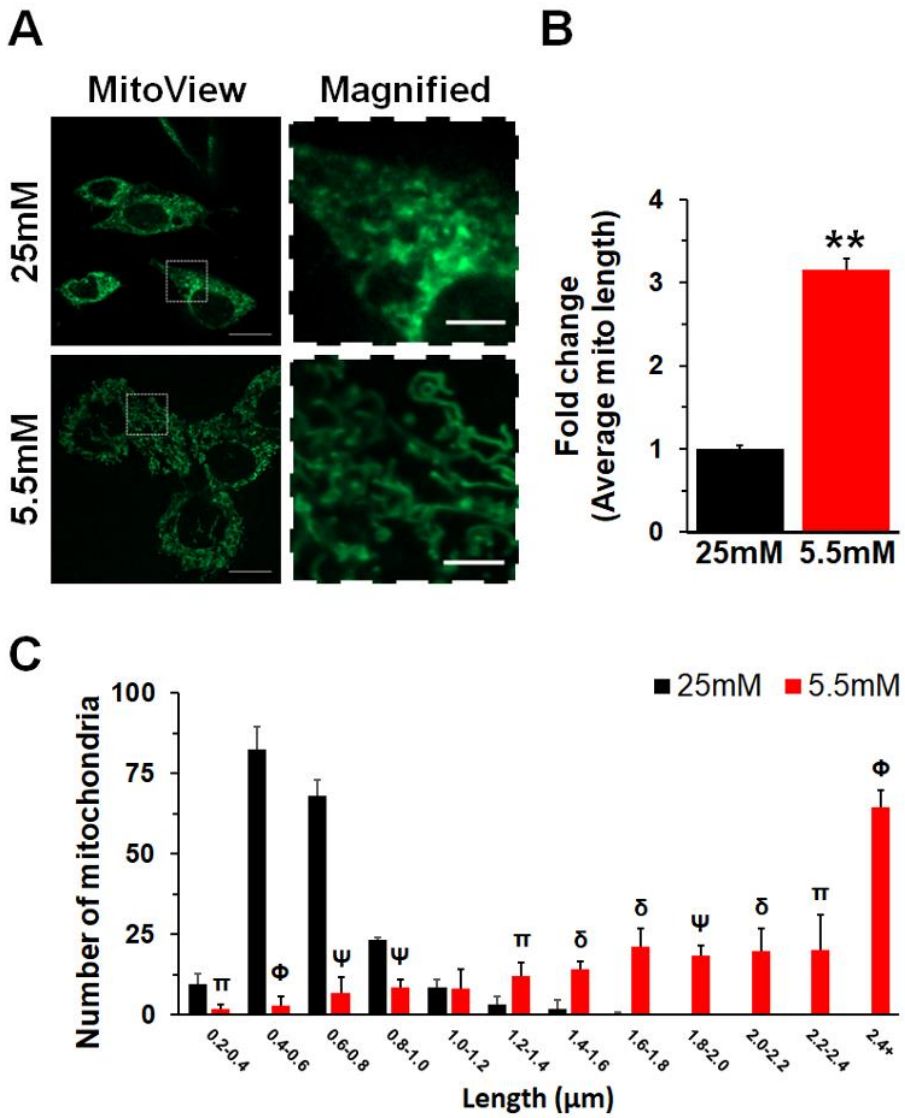

Figure 4.7. NAD$^+$/NADH ratio is associated with regulation of C2C12 mitochondrial morphology. (A) Representative confocal microscopy live cell images C2C12 mitochondria stained with MitoView Green cultured in 25mM or 5.5mM glucose. Magnified area presented is outlined with the dashed box on non-magnified picture. Scale bar = 20µm and 5µm, respectively. **(B)** Graphical representation of fold change in average mitochondrial length of C2C12 cells grown in 25mM or 5.5mM glucose using Image J quantification. n=3 clonal cell lines. Two-tailed unpaired Student T-test, **p<0.01. **(C)** Graphical representation for number of mitochondria per grouped lengths using Image J quantification. Two-tailed unpaired Student T-test, π=*p<0.05, δ=**p<0.01, Ψ=***p<0.001, Φ=****p<0.0001.

Figure 4.8

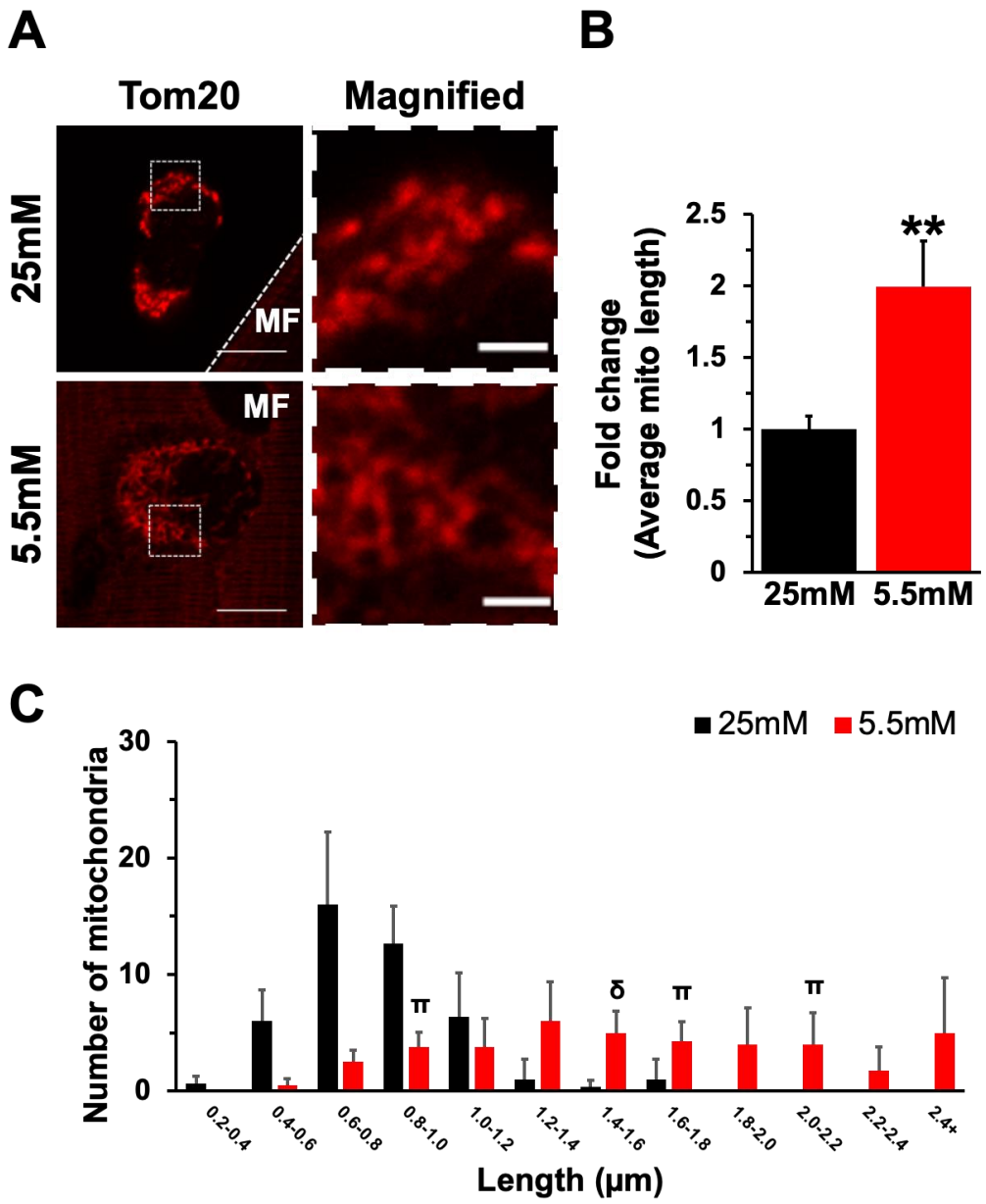

Figure 4.8. NAD$^+$/NADH ratio is associated with regulation of SC mitochondrial morphology. (A) Representative confocal immunohistochemistry for Tom20 of SCs cultured in 25mM or 5.5mM glucose. Magnified area presented is outlined with the dashed box on non-magnified picture. Scale bar = 10μm and 2μm, respectively. MF denotes the area occupied by the myofiber. **(B)** Graphical representation of fold change in average mitochondrial length of SCs grown in 25mM or 5.5mM glucose using Image J quantification. n=4 mice. Two-tailed unpaired Student T-test, **p <0.01. **(C)** Graphical representation for number of mitochondria per grouped lengths using Image J quantification. Two-tailed unpaired Student T-test, π=*p<0.05, δ=**p<0.01.

Figure 4.9

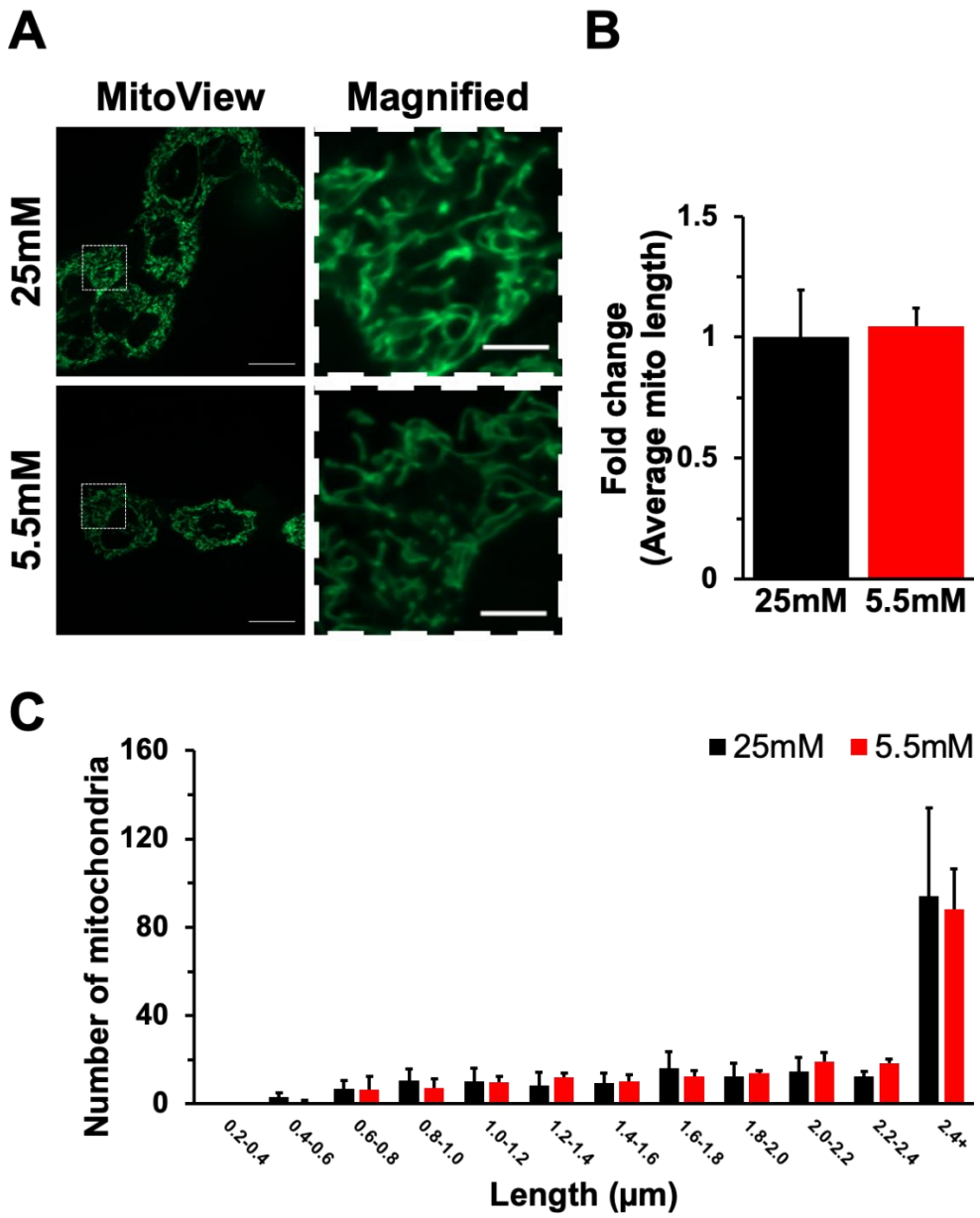

Figure 4.9. p107KO C2C12 cells display no changes in mitochondrial morphology when grown in disparate glucose concentrations. (A) Representative confocal microscopy live cell images of stained mitochondria (MitoView Green) for C2C12 cells cultured in 25mM or 5.5mM glucose. Magnified area presented is outlined with the dashed box on non-magnified picture. Scale bar = 20μm and 5μm, respectively. MF denotes the area occupied by the myofiber. **(B)** Graphical representation of fold change in average mitochondrial length of cells grown in 25mM or 5.5mM glucose using Image J quantification. n=3 clonal cell lines. **(C)** Graphical representation of number of mitochondria per grouped lengths using Image J quantification.

Figure 4.10

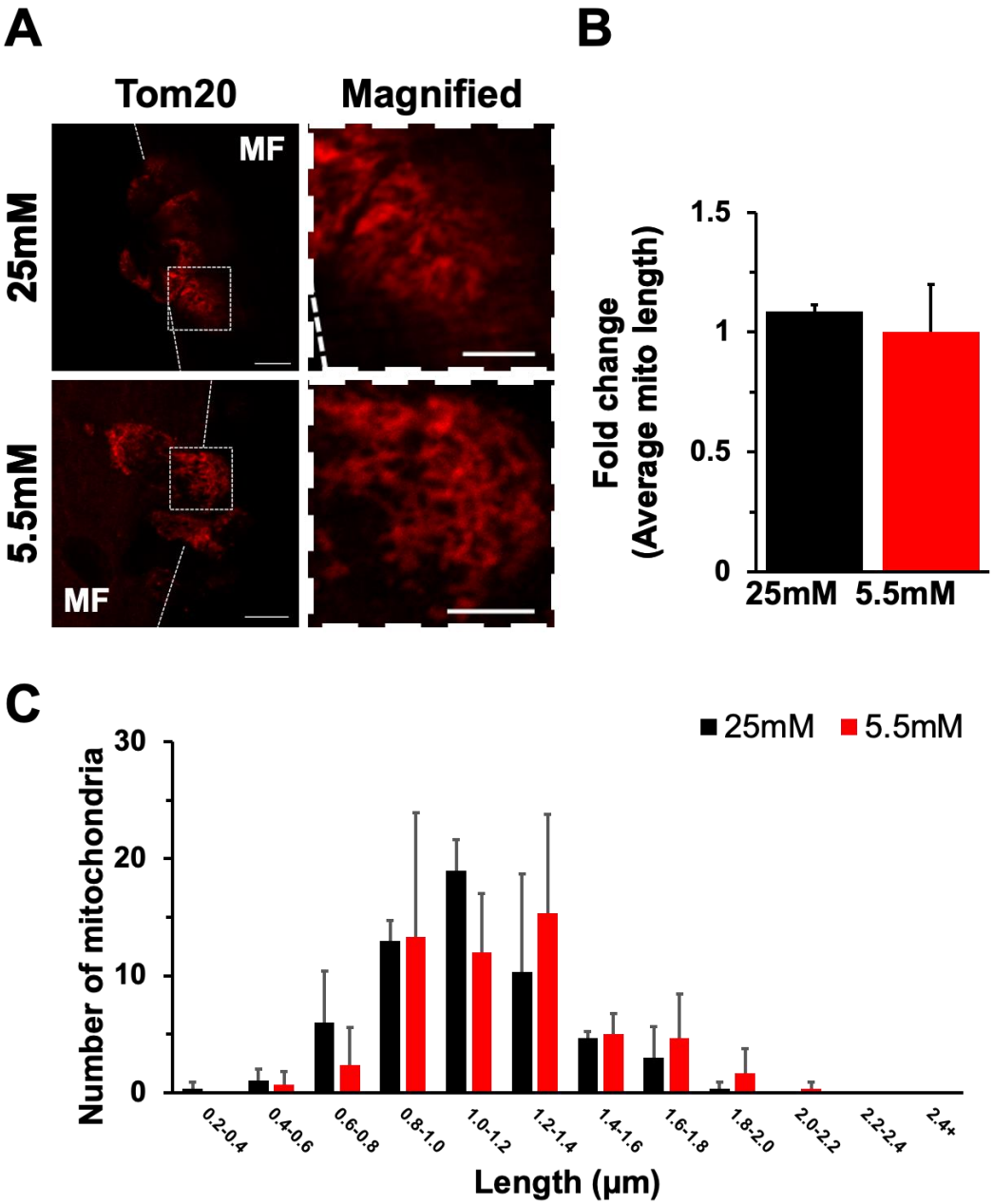

Figure 4.10. p107KO SCs display no changes in mitochondrial morphology when grown in disparate glucose concentrations. (A) Representative confocal immunohistochemistry for Tom20 p107KO SCs cultured in 25mM or 5.5mM glucose. Magnified area presented is outlined with the dashed box on non-magnified picture. Scale bar = 10μm and 5μm, respectively. **(B)** Graphical representation of fold change in average mitochondrial length of cells grown in 25mM or 5.5mM glucose using Image J quantification. n=4 mice. **(C)** Graphical representation of mitochondria number per grouped lengths using Image J quantification.

Figure 4.11

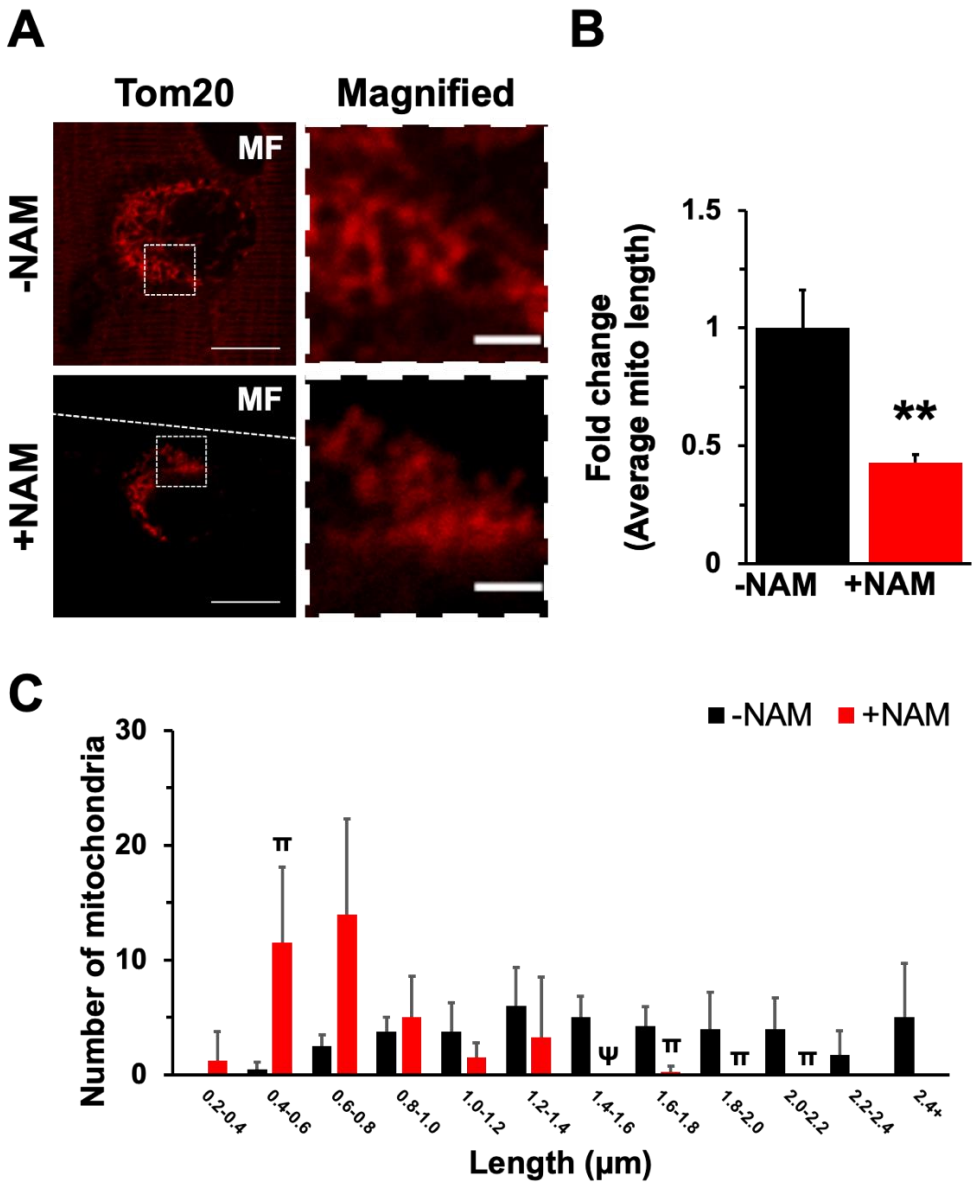

Figure 4.11. Sirt activity affects mitochondrial network organization of SCs. (A) Representative confocal immunohistochemistry for Tom20 SCs cultured in 5.5mM glucose supplemented with and without NAM. Magnified area presented is outlined with the dashed box on non-magnified picture. Scale bar = 10μm and 2μm, respectively. MF denotes the area occupied by the myofiber. **(B)** Graphical representation of fold change in average mitochondrial length under varying glucose conditions, using Image J quantification. n=4 mice. Two-tailed unpaired Student T-test, **p <0.01. **(C)** Graphical representation of mitochondria number per grouped lengths using Image J quantification. Two-tailed unpaired Student T-test, π=*p<0.05, Ψ=***p<0.001.

Figure 4.12

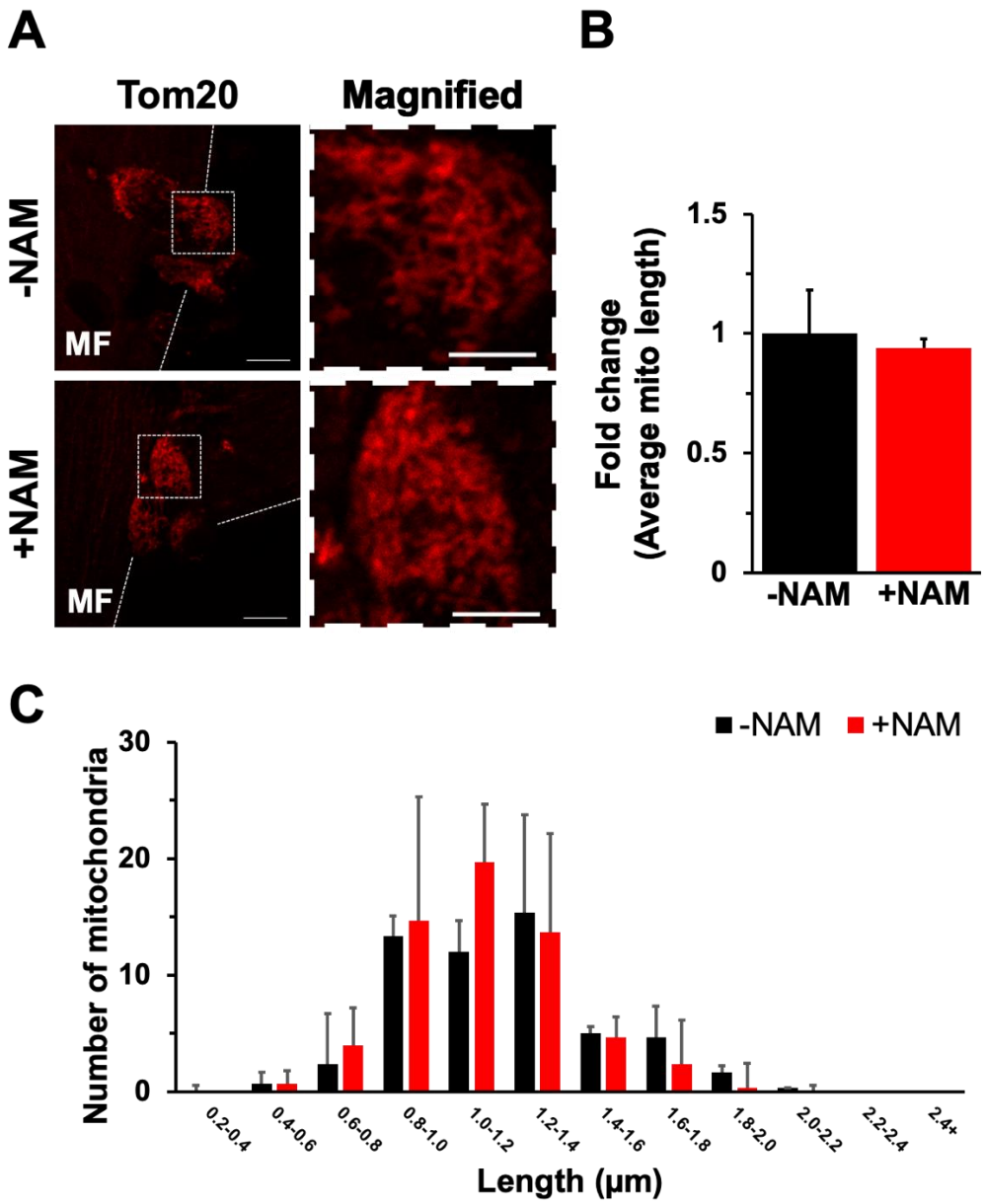

Figure 4.12. p107KO SC mitochondria network organization is not affected by NAM mediated Sirt inhibition. (A) Representative confocal immunohistochemistry for Tom20 p107KO SCs cultured in 5.5mM glucose in the absence or presence of NAM. Magnified area presented is outlined with the dashed box on non-magnified picture. Scale bar = 10µm and 5µm, respectively. **(B)** Graphical representation of fold change in average mitochondrial length of cells grown in 25mM or 5.5mM glucose, using Image J quantification. n=4 mice. **(C)** Graphical representation of mitochondria number per grouped lengths and areas using Image J quantification. Two-tailed unpaired Student T-test concludes no statistical significance between any groups.

Figure 4.13

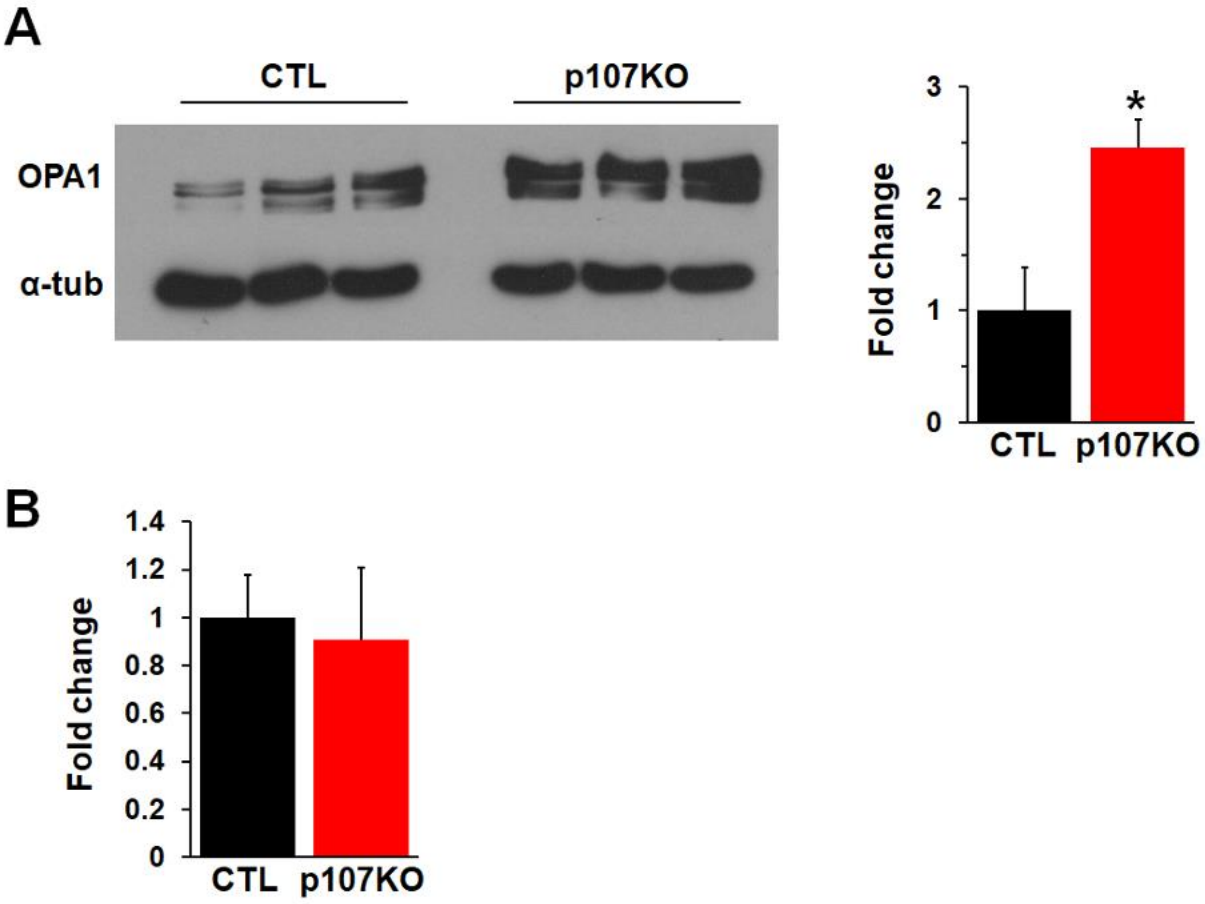

Figure 4.13. p107KO C2C12 cells have higher protein levels of OPA1. (A) Representative Western blot of OPA1 and α-tubulin (α-tub) for control (CTL) and p107KO C2C12 cells and graphical representation of OPA1 protein expression. n=3 clonal cell lines. Two tailed unpaired t-test, *$p < 0.05$. (B) RT-qPCR analysis of OPA1 gene expression for CTL and p107KO C2C12 cells. n=3 clonal cell lines.

Figure 4.14

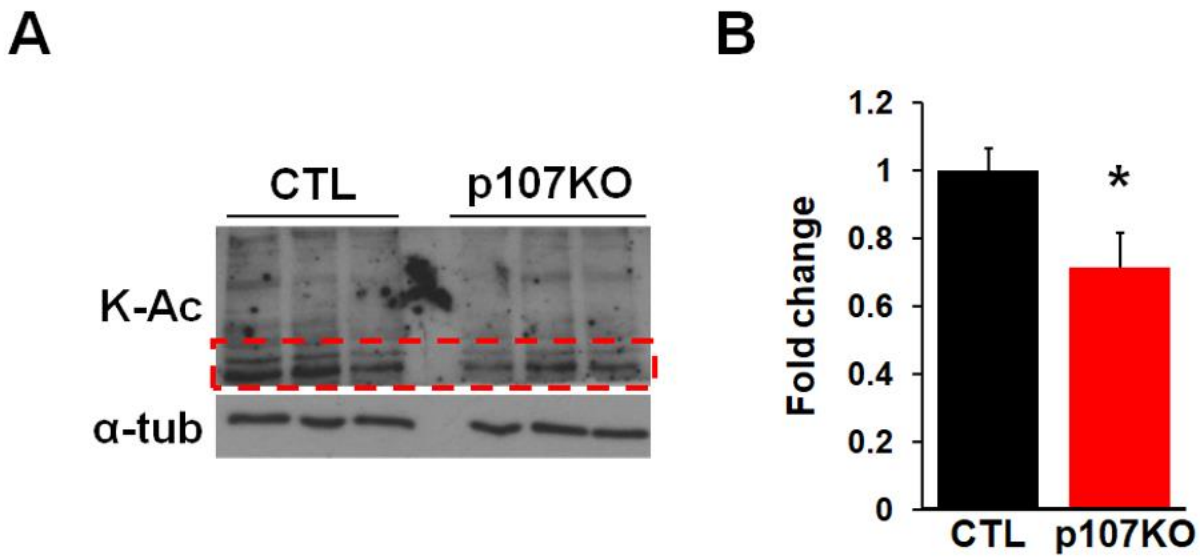

Figure 4.14. p107KO C2C12 cells have lower levels of protein acetylation. (A) Representative Western blot of acetylated protein lysine residues (K-Ac) above 75kDa in weight and α-tubulin for control C2C12 and p107KO cells. (B) Densitometric analysis of area outlined by hashed lines in (A). n=3 clonal cell lines. Two tailed unpaired t-test, *$p < 0.05$.

CHAPTER 5

DISCUSSION

Adult skeletal muscle stem cell (SC) dysfunction is known to be associated with muscle wasting diseases and other impairments in regenerative function, such as in muscular dystrophies and age-related sarcopenia (Chang et al., 2016; Dumon et al., 2015; Tieland et al., 2018). Thus, a deeper understanding of the mechanisms that control SC fate decisions could provide insight and possible therapeutic targets to correct the imbalance. While we had previously published a mitochondrial role for p107 in the myogenic cell line C2C12 (Bhattacharya et al., 2021), we had not fully explored this role in SCs. Now we find, through a well-established myofiber explant approach, that p107 also has a mitochondrial role in SC fate decisions. Similar to the in vitro studies with C2C12 cells, we find that p107 localization in SCs is manipulated by glucose availability that regulates the NAD^+/NADH ratio. We show that p107 is localized to the mitochondria in growth with 25mM glucose (**Fig. 4.1**) and conversely, when grown in 5.5mM glucose conditions, p107 is mostly localized outside of the mitochondria (**Fig. 4.2**). Moreover, our findings indicate that p107 subcellular localization is controlled by Sirt activity in SCs (**Fig. 4.3 and Fig. 4.4**). Indeed, inhibition of Sirt activity with NAM causes p107 to localize to the mitochondria when grown in 5.5mM glucose to a similar extent as when grown in 25mM glucose (**Fig. 4.3 and Fig. 4.4**). Importantly, our results show that mitochondrial localization of p107 potentially forces SC fates in favor of commitment to differentiation rather than self-renewal (**Fig. 4.4**). The role of p107 regulation of SC fate decisions was confirmed by showing that p107KO SCs displayed no differences in their fate decisions when altering glucose concentration or in the

presence of NAM (**Fig. 4.5**). These findings highlight how glucose control of the NAD^+/NADH ratio can affect Sirt activity, which controls p107 localization (**Fig 5.1**).

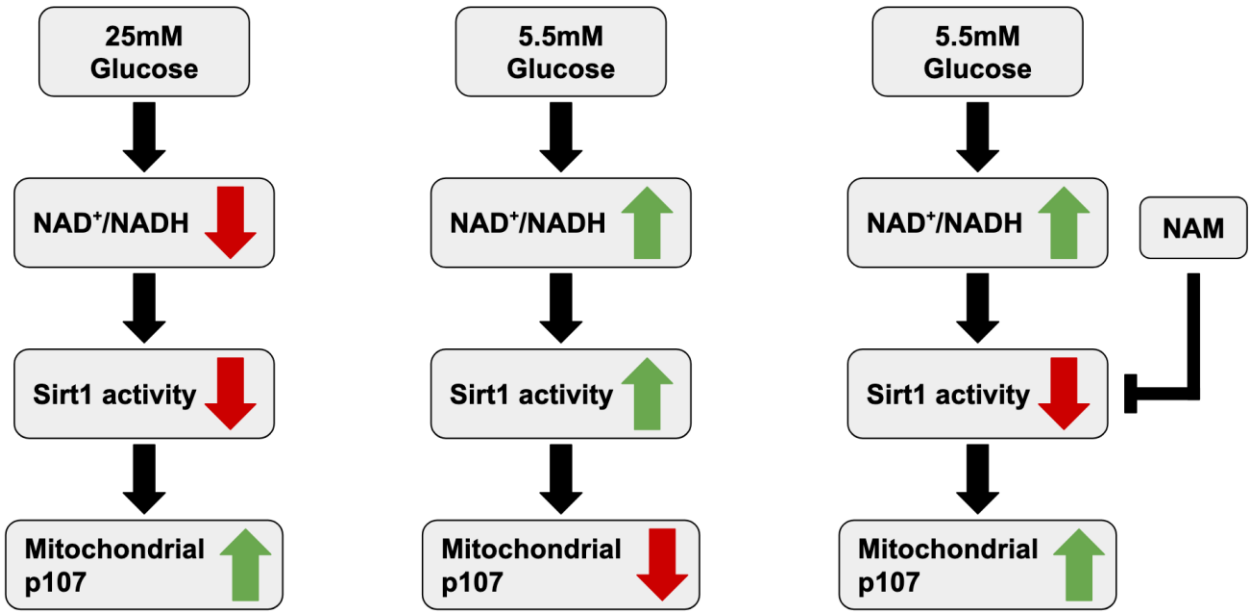

Figure 5.1. Various treatments and their effects on p107 mitochondrial localization. The localization of p107 can be influenced by changes to sirtuin activity, which itself is regulated by the NAD^+/NADH ratio of the cell. By influencing the NAD^+/NADH ratio, p107 localization can be changed, however this effect is dependent on sirtuin activity.

Interestingly, confocal immunofluorescence for p107 shows that it was never found localized to the nucleus of SCs, in any glucose growth condition (**Fig. 4.1**). This result contradicts the common belief that p107 functions in the nucleus in all cell types, as previous assessments are almost exclusively based on cancer cell lines (Wirt and Sage, 2010). It might describe a non-nuclear mitochondrial functional role for p107 that is strictly applicable to SCs, as p107 is found in the nucleus of the myoblast cell line C2C12 (Bhattacharya et al., 2021). This highlights the deficiency of using cell lines, such as C2C12 cells, to model for SC behaviour. Notably, it emphasizes a potential drawback in using cell lines to accurately understand p107 function. The difference between SCs and cell lines might reflect the absence of a micro niche in the latter that

the primary SCs are privy to on the myofiber (Yin et al., 2013). As the niche provides support and signaling to SCs, the lack of the myofiber environment in C2C12 cells could contribute to differential phenotypic character and gene functioning (Yin et al., 2013). By describing a function in the mitochondria, these new findings for p107 underscore its non-canonical non-nuclear role in SCs.

We believe that the sirtuin that regulates p107 mitochondrial localization is Sirt1, as it was shown in C2C12 cells that p107 interacted directly with Sirt1, and that inhibition of Sirt activity specifically prevented p107 from entering the mitochondria (Bhattacharya et al., 2021). We also inhibited SC Sirt activity with NAM, to test if it influenced p107 localization (**Fig. 4.3**). However, as NAM is an indiscriminate sirtuin inhibitor (Rymarchyk et al., 2021), to properly establish the role of Sirt1 in the p107 mitochondrial pathway, we would have to specifically inhibit and activate Sirt1 without affecting the other sirtuins. This can be accomplished in a variety of approaches. For example, Selisistat, the only selective Sirt1 inhibitor to enter human drug trials, offers a chemical method to selectively inhibit Sirt1 in SCs (Westerberg et al., 2015). Alternatively, SCs in myofiber culture can be transfected with Crispr/Cas9 to genetically delete Sirt1, or with Sirt1 interfering RNA (RNAi) to attenuate Sirt1 translation. To specifically activate Sirt1 SCs on myofibers in culture can be treated with Sirt1 specific activators, such as srt1720 (Minor et al., 2011).

It was recently found that another sirtuin, Sirt2, has been implicated in increasing SC self-renewal, in this case through the deacetylation of Pax7 (Sincennes et al., 2021). This might suggest that Sirt2 is the actual target in SCs when treated with NAM to force commitment to differentiation (**Fig. 4.5**). Nonetheless, as p107KO SCs displayed no changes in fate decisions when treated with NAM, it indicated that Sirt1 or Sirt2 is dependent on p107. Evaluating SC fate decisions by specifically activating Sirt1 or Sirt2 in p107KO SCs should discriminate which Sirt requires p107's

function. To definitively test if p107 mitochondrial function causes SC fate decision to commit to differentiate instead of self-renewal, p107 could be re-introduced by a plasmid encoding for mitochondrially targeted p107 specifically into the mitochondria p107KO SCs (Bhattacharya et al., 2021). The specific mitochondrial expression of p107 in the p107KO cells should rescue the self-renewal phenotype. Furthermore, to effectively establish a downstream of Sirt function, transfection combined with the NAM treatment will corroborate if Sirt function is dependent on the presence of p107 if the rescue effects are eliminated.

p107 potentially influences SC fate decisions by regulating mitochondrial dynamics, which is associated with directing SC fate decisions (Baker et al., 2022). Results in C2C12 and SCs cells showed that p107 mitochondrial localization is associated with mitochondrial fragmentation (**Fig. 4.6 and Fig. 4.7**). Importantly, p107KO C2C12 cells and p107KO SCs exhibit highly connected mitochondrial network despite varying the NAD+/NADH ratio with glucose (**Fig. 4.9 and Fig. 4.10**), suggesting a p107 role in mitochondrial dynamics. This is further strengthened by inhibition of Sirt activity using NAM in SCs, which causes p107 to localize to the mitochondria and resulted in higher rates of mitochondrial fragmentation (**Fig. 4.8**), whereas p107KO SCs maintained a highly interconnected network in the presence of NAM (**Fig. 4.11**).

As p107KO SCs displayed significant higher levels of mitochondrial interconnectivity, it suggested that OPA1 activity, a protein facilitating mitochondrial fusion, might be augmented (Tilokani et al., 2018). Western blotting analysis of OPA1 protein levels between control and p107KO C2C12 cells showed that p107KO cells had significantly higher levels than controls (**Fig. 4.12A**). The high protein levels did not correlate with OPA1 gene expression levels, which were not different (**Fig. 4.12B**), suggesting a potential post-translational regulatory effect of OPA1 in p107KO cells to maintain the higher levels. As OPA1 deacetylation is known to enhance its

activity (Samant et al., 2014), OPA1 activity might be linked to cellular protein acetylation levels in p107KO SCs (Samant et al., 2014). Indeed, compared to controls, p107KO cells displayed a notable decrease in global cellular acetylation rates (**Fig. 4.13**), signifying that p107 mitochondrial function might impact OPA1 acetylation status and hence its activity. Together, these results suggest that p107 mitochondrial function might affect mitochondrial structure, possibly through OPA1, which affects SC fate decision making (Baker et al., 2022).

The importance of the phenotypic change in the mitochondrial network is that mitochondrial activity has been identified as a key mediator in the maintenance of SC quiescence and self-renewal (Baker et al., 2022; Hong et al., 2022; Ito and Ito, 2016). Mitochondrial dynamics are important in cellular metabolism, as the structure of the mitochondria determines in part their efficiency and oxidative potential, with higher interconnectivity generally being associated with higher Oxphos levels (Mitra et al., 2009; Hoitzing et al., 2015, Gomes et al., 2011). Previous work in C2C12 cells established that p107KO cells had a pro-oxidative phenotype associated with increased mitochondrial interconnectivity (Bhattacharya et al., 2021). Crucially, increases in mitochondrial interconnectivity has recently been shown to increase self-renewal rates in SCs (Baker et al., 2022). This suggests that p107 mitochondrial function might regulate SC fate decisions through its control of mitochondrial dynamics affecting metabolism. However, SC metabolism has yet to be assessed. An indirect approach to address the metabolic profile in SCs when p107 is present or removed from the mitochondria would be to determine the global transcriptome to find if genes associated with Oxphos are downregulated when p107 is present in the mitochondria (Hong et al., 2022). Alternatively, the metabolome could be assessed to observe changes in cellular nutrient shuttling between p107KO and WT cells (Weckmann et al., 2018; Kumar et al., 2020).

Though we observe a correlation between the absence of p107 and increased OPA1 levels and mitochondrial fusion, the causation for this correlation is unknown, suggestive that novel p107 interacting proteins might facilitate the differences OPA1 levels. We can use a proteome analysis to find potential p107 interacting proteins. For this, we can immunoprecipitate WT and p107KO primary myoblast lysates for p107, wash the immune complex to remove nonspecific binding, and then disrupt the p107 immune complexes. Using mass spectrometry analysis, we can then analyze the proteins present in the immune complexes. The identity of the interacting proteins are determined by eliminating any found in the negative control p107KO lysates from those that are present in WT lysates. In turn, we could then study these interacting proteins by their over expression or inhibition to determine their effect on SC fate transitions, OPA1 levels, and mitochondrial dynamics in WT and p107KO SCs. This might allow us to potentially establish which proteins are upstream or downstream effectors of p107 function.

We propose that p107 might be acting in a multifaceted mechanism that contributes to the cellular acetylome to activate genes related to self-renewal. In SCs, there is evidence to suggest that lower levels of protein acetylation, and enhanced deacetylation promotes self-renewal (Ryall et al., 2015). We found that p107KO cells possess lower levels of cellular acetylation, suggesting that this mechanism may be in effect (**Fig. 4.14**). Though p107 is kept from the mitochondria by the high NAD^+/NADH ratio, the absence of p107 in the mitochondria of SCs would also increase the NAD^+/NADH ratio by increasing Oxphos efficiency in a feed forward mechanism. The result is an enhanced Sirt activity, which would affect cellular acetylation levels (Ryall et al., 2014; Kupis et al., 2016). Indeed, stem cells tend to generally down-regulate acetylation related activity as they return to quiescence (Moussaieff et al., 2015; Lee et al., 2014). Also, while Pax7 activity affects SC fate choices, new evidence shows that it can also be regulated through protein acetylation. Pax7

activity was found to increase when deacetylated, which was performed by Sirt2, and can be stimulated by a high NAD^+/NADH ratio (Sincennes et al., 2021). Thus, p107 may be implicated in the epigenetic regulation of SC fate decisions through its control over cellular NAD+/NADH ratios, which affect Sirt activity.

The reduction in global acetylation may indicate a role for p107 in epigenetic regulation that would impact SC fate decisions. Ryall et al. demonstrated that Sirt1 function is important in preventing SC commitment genes from being expressed, by suppressing their acetylation status (Ryall et al., 2015). Indeed, epigenetic regulation by histone deacetylase activity at the Myod1 promotor is known to affect fate decisions, causing preference for self-renewal as MyoD is repressed (Puri et al., 2001; Massenet et al., 2021). Conversely, the association of histone acetyltransferases (HATs), in particular p300, at the Myod1 promotor increases MyoD expression and subsequent differentiation (Hamed et al., 2013). Hence, the reduction in acetylation in p107KO cells (**Fig. 4.14**), suggests that the removal of p107 causes an increase in histone deacetylase activity as well as a decrease in acetyltransferase activity. This would affect SC fate decisions through the modulation of the Myod1 gene, which encodes for MyoD, one of the master myogenic differentiation factors.

Though Sirt deacetylase activity was established through the analysis of the NAD^+/NADH ratio (Bhattacharya et al., 2021), HAT activity has not yet been analyzed in in the absence or presence of p107. We propose that the metabolic influence of p107 not only contributes to the NAD^+/NADH ratio, but might influence the availability of acetyl-CoA, in turn regulating HAT activity. The activity of histone acetyltransferases is controlled by many factors, though one such mechanism of control is the availability of necessary metabolites, in this case, acetyl-CoA (Legube and Trouche, 2003). Determining acetyl-CoA availability can be done through commercially

available acetyl-CoA assay kits, or through mass spectrometry analysis of acetyl-CoA in tandem with previously mentioned metabolomics. To assay for larger epigenetic modifications of SCs and determine which genes differ in epigenetic regulation between the p107KO and WT cells, we could sequence the genes that are actively expressed in the cells using transposase-accessible chromatin using sequencing (ATAC-seq), an approach that has been recently refined for SCs (Dong et al., 2023).

In summary, our findings establish that p107 might regulate SC fate decisions that is associated with changes in mitochondrial remodeling and possibly acts through the mitochondrial fusion protein OPA1. We reveal that this effect on SCs acts in a Sirt dependent manner, with the localization of p107 being dictated by the activity of Sirts and suggest Sirt1 as a likely candidate. When sequestered in the mitochondria, p107 acts to shift SCs towards commitment, while its localization outside of the mitochondria causes a preference for self-renewal. We propose a that the possible mechanism of action for SC fate decisions is through control over cellular acetylation levels, which may in turn epigenetically regulate quiescence and self-renewal genes. While this avenue remains to be explored, it nevertheless establishes p107 as a novel regulator of SC self-renewal, possibly implicating it as a target to combat SC related muscle degenerative diseases.

CHAPTER 6

FUTURE DIRECTION

To further our understanding of p107 and characterize its function in SCs, it would be important to determine a specific inhibitor of p107, as none exist currently. This can be potentially accomplished by first ascertaining the modifications or domains that are responsible for p107 mitochondrial localization, and hence its mitochondrial role to promote commitment over self-renewal. Furthermore, the binding partner for p107 in the mitochondria has never been identified, though it has previously been suggested to be E2F4 (Bhattacharya et al., 2021). Elucidating these interactions can help with the creation of a p107 specific inhibitor, which could potentially serve to influence SC fate decisions in vivo and allow for further experimentation on pathways involved in SC fates.

Additionally, it would be of great interest to explore the transcriptome of p107KO compared to control SCs. Analysis of the cellular transcriptome would provide insight into molecular pathways affected by p107 in SCs, potentially reinforcing our current findings and shedding light on new directions for p107 research. Finally, a shortcoming of our p107KO mouse model is that it is a whole-body knockout, where p107 is absent in all body tissues and during growth and development. While these mice display no developmental defects or differences compared to their age matched control litter mates, it would nevertheless be prudent to use p107 loxp mice to specifically remove p107 in SCs. This would eliminate any potential developmental input of p107 in SCs and also exclude the potential of p107 deleted cells affecting SC behaviour.

CHAPTER 7

REFERENCES

Anand, R., Wai, T., Baker, M. J., Kladt, N., Schauss, A. C., Rugarli, E., & Langer, T. (2014). The i-AAA protease YME1L and OMA1 cleave OPA1 to balance mitochondrial fusion and fission. *Journal of Cell Biology*, *204*(6), 919–929. https://doi.org/10.1083/jcb.201308006

Arnold, P. K., & Finley, L. W. S. (2023). Regulation and function of the mammalian tricarboxylic acid cycle. *The Journal of Biological Chemistry*, *299*(2), 102838. https://doi.org/10.1016/j.jbc.2022.102838

Baker, N., Wade, S., Triolo, M., Girgis, J., Chwastek, D., Larrigan, S., Feige, P., Fujita, R., Crist, C., Rudnicki, M. A., Burelle, Y., & Khacho, M. (2022). The mitochondrial protein OPA1 regulates the quiescent state of adult muscle stem cells. *Cell Stem Cell*, *29*(9), 1315-1332.e9. https://doi.org/10.1016/j.stem.2022.07.010

Basu, U., Bostwick, A. M., Das, K., Dittenhafer-Reed, K. E., & Patel, S. S. (2020). Structure, mechanism, and regulation of mitochondrial DNA transcription initiation. *The Journal of Biological Chemistry*, *295*(52), 18406–18425. https://doi.org/10.1074/jbc.REV120.011202

Bhattacharya, D., & Scimè, A. (2020). Mitochondrial Function in Muscle Stem Cell Fates. In *Frontiers in Cell and Developmental Biology* (Vol. 8, p. 480). https://www.frontiersin.org/article/10.3389/fcell.2020.00480

Bhattacharya, D., Shah, V., Oresajo, O., & Scimè, A. (2021). p107 mediated mitochondrial function controls muscle stem cell proliferative fates. *Nature Communications*, *12*(1), 5977. https://doi.org/10.1038/s41467-021-26176-0

Bjornson, C. R. R., Cheung, T. H., Liu, L., Tripathi, P. V, Steeper, K. M., & Rando, T. A. (2012). Notch Signaling Is Necessary to Maintain Quiescence in Adult Muscle Stem Cells. *Stem Cells*, *30*(2), 232–242. https://doi.org/10.1002/stem.773

Brun, C. E., Sincennes, M.-C., Lin, A. Y. T., Hall, D., Jarassier, W., Feige, P., Le Grand, F., & Rudnicki, M. A. (2022). GLI3 regulates muscle stem cell entry into G(Alert) and self-renewal. *Nature Communications*, *13*(1), 3961. https://doi.org/10.1038/s41467-022-31695-5

Brun, C. E., Wang, Y. X., & Rudnicki, M. A. (2018). *Single EDL Myofiber Isolation for Analyses of Quiescent and Activated Muscle Stem Cells BT - Cellular Quiescence: Methods and Protocols* (H. D. Lacorazza (ed.); pp. 149–159). Springer New York. https://doi.org/10.1007/978-1-4939-7371-2_11

Chang, N. C., Chevalier, F. P., & Rudnicki, M. A. (2016). Satellite Cells in Muscular Dystrophy - Lost in Polarity. *Trends in Molecular Medicine*, *22*(6), 479–496. https://doi.org/10.1016/j.molmed.2016.04.002

Chang, N. C., Sincennes, M.-C., Chevalier, F. P., Brun, C. E., Lacaria, M., Segalés, J., Muñoz-Cánoves, P., Ming, H., & Rudnicki, M. A. (2018). The Dystrophin Glycoprotein Complex Regulates the Epigenetic Activation of Muscle Stem Cell Commitment. *Cell Stem Cell*, *22*(5), 755-768.e6. https://doi.org/10.1016/j.stem.2018.03.022

Chen, D., Livne-bar, I., Vanderluit, J. L., Slack, R. S., Agochiya, M., & Bremner, R. (2004). Cell-specific effects of RB or RB/p107 loss on retinal development implicate an intrinsically death-resistant cell-of-origin in retinoblastoma. *Cancer Cell*, *5*(6), 539–551. https://doi.org/10.1016/j.ccr.2004.05.025

Chen, H., Chomyn, A., & Chan, D. C. (2005). Disruption of Fusion Results in Mitochondrial Heterogeneity and Dysfunction. *Journal of Biological Chemistry*, *280*(28), 26185–26192. https://doi.org/10.1074/jbc.M503062200

Chen, H., Vermulst, M., Wang, Y. E., Chomyn, A., Prolla, T. A., McCaffery, J. M., & Chan, D. C. (2010). Mitochondrial fusion is required for mtDNA stability in skeletal muscle and tolerance of mtDNA mutations. *Cell*, *141*(2), 280–289. https://doi.org/10.1016/j.cell.2010.02.026

Cogliati, S., Frezza, C., Soriano, M. E., Varanita, T., Quintana-Cabrera, R., Corrado, M., Cipolat, S., Costa, V., Casarin, A., Gomes, L. C., Perales-Clemente, E., Salviati, L., Fernandez-Silva, P., Enriquez, J. A., & Scorrano, L. (2013). Mitochondrial Cristae Shape Determines Respiratory Chain Supercomplexes Assembly and Respiratory Efficiency. *Cell*, *155*(1), 160–171. https://doi.org/10.1016/j.cell.2013.08.032

Cornelison, D. D. W., & Wold, B. J. (1997). Single-Cell Analysis of Regulatory Gene Expression in Quiescent and Activated Mouse Skeletal Muscle Satellite Cells. *Developmental Biology*, *191*(2), 270–283. https://doi.org/https://doi.org/10.1006/dbio.1997.8721

Crist, C. G., Montarras, D., & Buckingham, M. (2012). Muscle satellite cells are primed for myogenesis but maintain quiescence with sequestration of Myf5 mRNA targeted by microRNA-31 in mRNP granules. *Cell Stem Cell*, *11*(1), 118–126. https://doi.org/10.1016/j.stem.2012.03.011

De Micheli, A. J., Spector, J. A., Elemento, O., & Cosgrove, B. D. (2020). A reference single-cell transcriptomic atlas of human skeletal muscle tissue reveals bifurcated muscle stem cell populations. *Skeletal Muscle*, *10*(1), 19. https://doi.org/10.1186/s13395-020-00236-3

De Sousa, M., Porras, D. P., Perry, C. G. R., Seale, P., & Scimè, A. (2014). p107 is a crucial regulator for determining the adipocyte lineage fate choices of stem cells. *Stem Cells (Dayton, Ohio)*, *32*(5), 1323–1336. https://doi.org/10.1002/stem.1637

DeBerardinis, R. J., Lum, J. J., Hatzivassiliou, G., & Thompson, C. B. (2008). The biology of cancer: metabolic reprogramming fuels cell growth and proliferation. *Cell Metabolism*, *7*(1), 11–20. https://doi.org/10.1016/j.cmet.2007.10.002

Dong, A., Chan, I. T. C., & Cheung, T. H. (2023). ATAC-seq protocol for the profiling of chromatin accessibility of in situ fixed quiescent and activated muscle stem cells. *STAR Protocols*, *4*(3), 102376. https://doi.org/10.1016/j.xpro.2023.102376

Dumont, N. A., Bentzinger, C. F., Sincennes, M.-C., & Rudnicki, M. A. (2015a). Satellite Cells and Skeletal Muscle Regeneration. *Comprehensive Physiology*, 1027–1059. https://doi.org/https://doi.org/10.1002/cphy.c140068

Dumont, N. A., Wang, Y. X., von Maltzahn, J., Pasut, A., Bentzinger, C. F., Brun, C. E., & Rudnicki, M. A. (2015b). Dystrophin expression in muscle stem cells regulates their polarity and asymmetric division. *Nature Medicine*, *21*(12), 1455–1463. https://doi.org/10.1038/nm.3990

Fajas, L. (2013). Re-thinking cell cycle regulators: the cross-talk with metabolism. *Frontiers in Oncology*, *3*, 4. https://doi.org/10.3389/fonc.2013.00004

Folmes, C. D. L., Dzeja, P. P., Nelson, T. J., & Terzic, A. (2012). Metabolic Plasticity in Stem Cell Homeostasis and Differentiation. *Cell Stem Cell*, *11*(5), 596–606. https://doi.org/10.1016/j.stem.2012.10.002

Fulco, M., Cen, Y., Zhao, P., Hoffman, E. P., McBurney, M. W., Sauve, A. A., & Sartorelli, V. (2008). Glucose restriction inhibits skeletal myoblast differentiation by activating SIRT1 through AMPK-mediated regulation of Nampt. *Developmental Cell*, *14*(5), 661–673. https://doi.org/10.1016/j.devcel.2008.02.004

Fulco, M., Schiltz, R. L., Iezzi, S., King, M. T., Zhao, P., Kashiwaya, Y., Hoffman, E., Veech, R. L., & Sartorelli, V. (2003). Sir2 Regulates Skeletal Muscle Differentiation as a Potential Sensor of the Redox State. *Molecular Cell*, *12*(1), 51–62. https://doi.org/10.1016/S1097-2765(03)00226-0

Gomes, L. C., Di Benedetto, G., & Scorrano, L. (2011). During autophagy mitochondria elongate, are spared from degradation and sustain cell viability. *Nature Cell Biology*, *13*(5), 589–598. https://doi.org/10.1038/ncb2220

Goodman, C. A., Hornberger, T. A., & Robling, A. G. (2015). Bone and skeletal muscle: Key players in mechanotransduction and potential overlapping mechanisms. *Bone*, *80*, 24–36. https://doi.org/https://doi.org/10.1016/j.bone.2015.04.014

Grabowska, W., Sikora, E., & Bielak-Zmijewska, A. (2017). Sirtuins, a promising target in slowing down the ageing process. *Biogerontology*, *18*(4), 447–476. https://doi.org/10.1007/s10522-017-9685-9

Hamed, M., Khilji, S., Chen, J., & Li, Q. (2013). Stepwise acetyltransferase association and histone acetylation at the Myod1 locus during myogenic differentiation. *Scientific Reports*, *3*, 2390. https://doi.org/10.1038/srep02390

Henley, S. A., & Dick, F. A. (2012). The retinoblastoma family of proteins and their regulatory functions in the mammalian cell division cycle. *Cell Division*, *7*(1), 10. https://doi.org/10.1186/1747-1028-7-10

Hickson, R. C., Rennie, M. J., Conlee, R. K., Winder, W. W., & Holloszy, J. O. (1977). Effects of increased plasma fatty acids on glycogen utilization and endurance. *Journal of Applied Physiology*, *43*(5), 829–833. https://doi.org/10.1152/jappl.1977.43.5.829

Hoitzing, H., Johnston, I. G., & Jones, N. S. (2015). What is the function of mitochondrial networks? A theoretical assessment of hypotheses and proposal for future research. *BioEssays : News and Reviews in Molecular, Cellular and Developmental Biology*, *37*(6), 687–700. https://doi.org/10.1002/bies.201400188

Hong, X., Isern, J., Campanario, S., Perdiguero, E., Ramírez-Pardo, I., Segalés, J., Hernansanz-Agustín, P., Curtabbi, A., Deryagin, O., Pollán, A., González-Reyes, J. A., Villalba, J. M., Sandri, M., Serrano, A. L., Enríquez, J. A., & Muñoz-Cánoves, P. (2022). Mitochondrial dynamics maintain muscle stem cell regenerative competence throughout adult life by regulating metabolism and mitophagy. *Cell Stem Cell*, *29*(9), 1298-1314.e10. https://doi.org/10.1016/j.stem.2022.07.009

Hori, S., Hiramuki, Y., Nishimura, D., Sato, F., & Sehara-Fujisawa, A. (2019). PDH-mediated metabolic flow is critical for skeletal muscle stem cell differentiation and myotube formation during regeneration in mice. *FASEB Journal : Official Publication of the Federation of American Societies for Experimental Biology*, *33*(7), 8094–8109. https://doi.org/10.1096/fj.201802479R

Ishihara, N., Fujita, Y., Oka, T., & Mihara, K. (2006). Regulation of mitochondrial morphology through proteolytic cleavage of OPA1. *The EMBO Journal*, *25*(13), 2966–2977. https://doi.org/10.1038/sj.emboj.7601184

Ito, K., & Ito, K. (2016). Metabolism and the Control of Cell Fate Decisions and Stem Cell Renewal. *Annual Review of Cell and Developmental Biology*, *32*, 399–409. https://doi.org/10.1146/annurev-cellbio-111315-125134

Jheng, H.-F., Tsai, P.-J., Guo, S.-M., Kuo, L.-H., Chang, C.-S., Su, I.-J., Chang, C.-R., & Tsai, Y.-S. (2012). Mitochondrial fission contributes to mitochondrial dysfunction and insulin resistance in skeletal muscle. *Molecular and Cellular Biology*, *32*(2), 309–319. https://doi.org/10.1128/MCB.05603-11

Kane, D. A. (2014). Lactate oxidation at the mitochondria: a lactate-malate-aspartate shuttle at work. *Frontiers in Neuroscience*, *8*, 366. https://doi.org/10.3389/fnins.2014.00366

Karamanlidis, G., Lee, C. F., Garcia-Menendez, L., Kolwicz Jr., S. C., Suthammarak, W., Gong, G., Sedensky, M. M., Morgan, P. G., Wang, W., & Tian, R. (2013). Mitochondrial Complex I Deficiency Increases Protein Acetylation and Accelerates Heart Failure. *Cell Metabolism*, *18*(2), 239–250. https://doi.org/10.1016/j.cmet.2013.07.002

Khacho, M., Clark, A., Svoboda, D. S., Azzi, J., MacLaurin, J. G., Meghaizel, C., Sesaki, H., Lagace, D. C., Germain, M., Harper, M.-E., Park, D. S., & Slack, R. S. (2016). Mitochondrial Dynamics Impacts Stem Cell Identity and Fate Decisions by Regulating a Nuclear Transcriptional Program. *Cell Stem Cell*, *19*(2), 232–247. https://doi.org/10.1016/j.stem.2016.04.015

Kim, B., Kim, J.-S., Yoon, Y., Santiago, M. C., Brown, M. D., & Park, J.-Y. (2013). Inhibition of Drp1-dependent mitochondrial division impairs myogenic differentiation. *American Journal of Physiology-Regulatory, Integrative and Comparative Physiology*, *305*(8), R927–R938. https://doi.org/10.1152/ajpregu.00502.2012

Kuang, S., Kuroda, K., Grand, F. Le, & Rudnicki, M. A. (2007). Asymmetric self-renewal and commitment of satellite stem cells in muscle. *Cell*, *129*(5), 999–1010. https://doi.org/10.1016/j.cell.2007.03.044

Kumar, A., Kumar, Y., Sevak, J. K., Kumar, S., Kumar, N., & Gopinath, S. D. (2020). Metabolomic analysis of primary human skeletal muscle cells during myogenic progression. *Scientific Reports*, *10*(1), 11824. https://doi.org/10.1038/s41598-020-68796-4

Kupis, W., Pałyga, J., Tomal, E., & Niewiadomska, E. (2016). The role of sirtuins in cellular homeostasis. *Journal of Physiology and Biochemistry*, *72*(3), 371–380. https://doi.org/10.1007/s13105-016-0492-6

Lahmann, I., Bröhl, D., Zyrianova, T., Isomura, A., Czajkowski, M. T., Kapoor, V., Griger, J., Ruffault, P. L., Mademtzoglou, D., Zammit, P. S., Wunderlich, T., Spuler, S., Kühn, R., Preibisch, S., Wolf, J., Kageyama, R., & Birchmeier, C. (2019). Oscillations of MyoD and Hes1 proteins regulate the maintenance of activated muscle stem cells. *Genes and Development*, *33*(9–10), 524–535. https://doi.org/10.1101/gad.322818.118

Latil, M., Rocheteau, P., Châtre, L., Sanulli, S., Mémet, S., Ricchetti, M., Tajbakhsh, S., & Chrétien, F. (2012). Skeletal muscle stem cells adopt a dormant cell state post mortem and retain regenerative capacity. *Nature Communications*, *3*(1), 903. https://doi.org/10.1038/ncomms1890

LeCouter, J. E., Kablar, B., Hardy, W. R., Ying, C., Megeney, L. A., May, L. L., & Rudnicki, M. A. (1998). Strain-dependent myeloid hyperplasia, growth deficiency, and accelerated cell cycle in mice lacking the Rb-related p107 gene. *Molecular and Cellular Biology*, *18*(12), 7455–7465. https://doi.org/10.1128/MCB.18.12.7455

Leduc-Gaudet, J.-P., Hussain, S. N. A., Barreiro, E., & Gouspillou, G. (2021). Mitochondrial Dynamics and Mitophagy in Skeletal Muscle Health and Aging. *International Journal of Molecular Sciences*, *22*(15). https://doi.org/10.3390/ijms22158179

Lee, C. F., Chavez, J. D., Garcia-Menendez, L., Choi, Y., Roe, N. D., Chiao, Y. A., Edgar, J. S., Goo, Y. A., Goodlett, D. R., Bruce, J. E., & Tian, R. (2016). Normalization of NAD+ Redox Balance as a Therapy for Heart Failure. *Circulation*, *134*(12), 883–894. https://doi.org/10.1161/CIRCULATIONAHA.116.022495

Lee, H., Smith, S. B., Sheu, S.-S., & Yoon, Y. (2020). The short variant of optic atrophy 1 (OPA1) improves cell survival under oxidative stress. *The Journal of Biological Chemistry*, *295*(19), 6543–6560. https://doi.org/10.1074/jbc.RA119.010983

Lee, J. V., Carrer, A., Shah, S., Snyder, N. W., Wei, S., Venneti, S., Worth, A. J., Yuan, Z.-F., Lim, H.-W., Liu, S., Jackson, E., Aiello, N. M., Haas, N. B., Rebbeck, T. R., Judkins, A., Won, K.-J., Chodosh, L. A., Garcia, B. A., Stanger, B. Z., … Wellen, K. E. (2014). Akt-Dependent Metabolic Reprogramming Regulates Tumor Cell Histone Acetylation. *Cell Metabolism*, *20*(2), 306–319. https://doi.org/10.1016/j.cmet.2014.06.004

Legube, G., & Trouche, D. (2003). Regulating histone acetyltransferases and deacetylases. *EMBO Reports*, *4*(10), 944–947. https://doi.org/https://doi.org/10.1038/sj.embor.embor941

Lian, D., Chen, M.-M., Wu, H., Deng, S., & Hu, X. (2022). The Role of Oxidative Stress in Skeletal Muscle Myogenesis and Muscle Disease. *Antioxidants (Basel, Switzerland)*, *11*(4). https://doi.org/10.3390/antiox11040755

Livak, K. J., & Schmittgen, T. D. (2001). Analysis of relative gene expression data using real-time quantitative PCR and the 2(-Delta Delta C(T)) Method. *Methods (San Diego, Calif.)*, *25*(4), 402–408. https://doi.org/10.1006/meth.2001.1262

Lunt, S. Y., & Heiden, M. G. Vander. (2011). Aerobic glycolysis: meeting the metabolic requirements of cell proliferation. *Annual Review of Cell and Developmental Biology*, *27*, 441–464. https://doi.org/10.1146/annurev-cellbio-092910-154237

Martínez-Reyes, I., & Chandel, N. S. (2020). Mitochondrial TCA cycle metabolites control physiology and disease. *Nature Communications*, *11*(1), 102. https://doi.org/10.1038/s41467-019-13668-3

Massenet, J., Gardner, E., Chazaud, B., & Dilworth, F. J. (2021). Epigenetic regulation of satellite cell fate during skeletal muscle regeneration. *Skeletal Muscle*, *11*(1), 4. https://doi.org/10.1186/s13395-020-00259-w

Mauro, A. (1961). Satellite cell of skeletal muscle fibers. *The Journal of Biophysical and Biochemical Cytology*, *9*(2), 493–495. https://doi.org/10.1083/jcb.9.2.493

McFarlan, J. T., Yoshida, Y., Jain, S. S., Han, X.-X., Snook, L. A., Lally, J., Smith, B. K., Glatz, J. F. C., Luiken, J. J. F. P., Sayer, R. A., Tupling, A. R., Chabowski, A., Holloway, G. P., & Bonen, A. (2012). In Vivo, Fatty Acid Translocase (CD36) Critically Regulates Skeletal Muscle Fuel Selection, Exercise Performance, and Training-induced Adaptation of Fatty Acid Oxidation *. *Journal of Biological Chemistry*, *287*(28), 23502–23516. https://doi.org/10.1074/jbc.M111.315358

Minor, R. K., Baur, J. A., Gomes, A. P., Ward, T. M., Csiszar, A., Mercken, E. M., Abdelmohsen, K., Shin, Y.-K., Canto, C., Scheibye-Knudsen, M., Krawczyk, M., Irusta, P. M., Martín-Montalvo, A., Hubbard, B. P., Zhang, Y., Lehrmann, E., White, A. A., Price, N. L., Swindell, W. R., … de Cabo, R. (2011). SRT1720 improves survival and healthspan of obese mice. *Scientific Reports*, *1*, 70. https://doi.org/10.1038/srep00070

Mishra, P., & Chan, D. C. (2016). Metabolic regulation of mitochondrial dynamics. *Journal of Cell Biology*, *212*(4), 379–387. https://doi.org/10.1083/jcb.201511036

Mitra, K., Wunder, C., Roysam, B., Lin, G., & Lippincott-Schwartz, J. (2009). A hyperfused mitochondrial state achieved at G1-S regulates cyclin E buildup and entry into S phase. *Proceedings of the National Academy of Sciences of the United States of America*, *106*(29), 11960–11965. https://doi.org/10.1073/pnas.0904875106

Moss, F. P., & Leblond, C. P. (1970). NATURE OF DIVIDING NUCLEI IN SKELETAL MUSCLE OF GROWING RATS. *Journal of Cell Biology*, *44*(2), 459–461. https://doi.org/10.1083/jcb.44.2.459

Moussaieff, A., Rouleau, M., Kitsberg, D., Cohen, M., Levy, G., Barasch, D., Nemirovski, A., Shen-Orr, S., Laevsky, I., Amit, M., Bomze, D., Elena-Herrmann, B., Scherf, T., Nissim-Rafinia, M., Kempa, S., Itskovitz-Eldor, J., Meshorer, E., Aberdam, D., & Nahmias, Y. (2015). Glycolysis-Mediated Changes in Acetyl-CoA and Histone Acetylation Control the Early Differentiation of Embryonic Stem Cells. *Cell Metabolism*, *21*(3), 392–402. https://doi.org/10.1016/j.cmet.2015.02.002

Myers, M. J., Shepherd, D. L., Durr, A. J., Stanton, D. S., Mohamed, J. S., Hollander, J. M., & Alway, S. E. (2019). The role of SIRT1 in skeletal muscle function and repair of older mice. *Journal of Cachexia, Sarcopenia and Muscle*, *10*(4), 929–949. https://doi.org/10.1002/jcsm.12437

Nielsen, J., Gejl, K. D., Hey-Mogensen, M., Holmberg, H.-C., Suetta, C., Krustrup, P., Elemans, C. P. H., & Ørtenblad, N. (2017). Plasticity in mitochondrial cristae density allows metabolic capacity modulation in human skeletal muscle. *The Journal of Physiology*, *595*(9), 2839–2847. https://doi.org/https://doi.org/10.1113/JP273040

Parodi-Rullán, R. M., Chapa-Dubocq, X. R., & Javadov, S. (2018). Acetylation of Mitochondrial Proteins in the Heart: The Role of SIRT3. In *Frontiers in Physiology* (Vol. 9). https://www.frontiersin.org/articles/10.3389/fphys.2018.01094

Porras, D. P., Abbaszadeh, M., Bhattacharya, D., D'souza, N. C., Edjiu, N. R., Perry, C. G. R., & Scimè, A. (2017). p107 Determines a Metabolic Checkpoint Required for Adipocyte Lineage Fates. *Stem Cells*, *35*(5), 1378–1391. https://doi.org/10.1002/stem.2576

Puri, P. L., Iezzi, S., Stiegler, P., Chen, T.-T., Schiltz, R. L., Muscat, G. E. O., Giordano, A., Kedes, L., Wang, J. Y. J., & Sartorelli, V. (2001). Class I Histone Deacetylases Sequentially Interact with MyoD and pRb during Skeletal Myogenesis. *Molecular Cell*, *8*(4), 885–897. https://doi.org/10.1016/S1097-2765(01)00373-2

Rafelski, S. M. (2013). Mitochondrial network morphology: building an integrative, geometrical view. *BMC Biology*, *11*(1), 71. https://doi.org/10.1186/1741-7007-11-71

Reinecke, F., Smeitink, J. A. M., & van der Westhuizen, F. H. (2009). OXPHOS gene expression and control in mitochondrial disorders. *Biochimica et Biophysica Acta (BBA) - Molecular Basis of Disease*, *1792*(12), 1113–1121. https://doi.org/https://doi.org/10.1016/j.bbadis.2009.04.003

Relaix, F., Bencze, M., Borok, M. J., Der Vartanian, A., Gattazzo, F., Mademtzoglou, D., Perez-Diaz, S., Prola, A., Reyes-Fernandez, P. C., Rotini, A., & Taglietti. (2021). Perspectives on skeletal muscle stem cells. *Nature Communications*, *12*(1), 692. https://doi.org/10.1038/s41467-020-20760-6

Reznik, M. (1969). Thymidine-3H uptake by satellite cells of regenerating skeletal muscle. *The Journal of Cell Biology*, *40*(2), 568–571. https://doi.org/10.1083/jcb.40.2.568

Ribeiro, A. F., Souza, L. S., Almeida, C. F., Ishiba, R., Fernandes, S. A., Guerrieri, D. A., Santos, A. L. F., Onofre-Oliveira, P. C. G., & Vainzof, M. (2019). Muscle satellite cells and impaired late stage regeneration in different murine models for muscular dystrophies. *Scientific Reports*, *9*(1), 11842. https://doi.org/10.1038/s41598-019-48156-7

Rochard, P., Rodier, A., Casas, F., Cassar-Malek, I., Marchal-Victorion, S., Daury, L., Wrutniak, C., & Cabello, G. (2000). Mitochondrial Activity Is Involved in the Regulation of Myoblast Differentiation through Myogenin Expression and Activity of Myogenic Factors *. *Journal of Biological Chemistry*, *275*(4), 2733–2744. https://doi.org/10.1074/jbc.275.4.2733

Rocheteau, P., Gayraud-morel, B., Siegl-cachedenier, I., Blasco, M. A., & Tajbakhsh, S. (2012). A Subpopulation of Adult Skeletal Muscle Stem Cells Retains All Template DNA Strands after Cell Division. *Cell*, *148*(1–2), 112–125. https://doi.org/10.1016/j.cell.2011.11.049

Rodgers, J. T., King, K. Y., Brett, J. O., Cromie, M. J., Charville, G. W., Maguire, K. K., Brunson, C., Mastey, N., Liu, L., Tsai, C.-R., Goodell, M. A., & Rando, T. A. (2014). mTORC1 controls the adaptive transition of quiescent stem cells from G0 to G(Alert). *Nature*, *510*(7505), 393–396. https://doi.org/10.1038/nature13255

Rodier, G., Makris, C., Coulombe, P., Scime, A., Nakayama, K., Nakayama, K. I., & Meloche, S. (2005). p107 inhibits G1 to S phase progression by down-regulating expression of the F-box protein Skp2. *Journal of Cell Biology*, *168*(1), 55–66. https://doi.org/10.1083/jcb.200404146

Rossignol, R., Gilkerson, R., Aggeler, R., Yamagata, K., Remington, S. J., & Capaldi, R. A. (2004). Energy Substrate Modulates Mitochondrial Structure and Oxidative Capacity in Cancer Cells. *Cancer Research*, *64*(3), 985–993. https://doi.org/10.1158/0008-5472.CAN-03-1101

Ryall, J. G., Dell'Orso, S., Derfoul, A., Juan, A., Zare, H., Feng, X., Clermont, D., Koulnis, M., Gutierrez-Cruz, G., Fulco, M., & Sartorelli, V. (2015). The NAD(+)-dependent SIRT1 deacetylase translates a metabolic switch into regulatory epigenetics in skeletal muscle stem cells. *Cell Stem Cell*, *16*(2), 171–183. https://doi.org/10.1016/j.stem.2014.12.004

Rymarchyk, S., Kang, W., & Cen, Y. (2021). Substrate-Dependent Sensitivity of SIRT1 to Nicotinamide Inhibition. *Biomolecules*, *11*(2). https://doi.org/10.3390/biom11020312

Samant, S. A., Zhang, H. J., Hong, Z., Pillai, V. B., Sundaresan, N. R., Wolfgeher, D., Archer, S. L., Chan, D. C., & Gupta, M. P. (2014). SIRT3 deacetylates and activates OPA1 to regulate mitochondrial dynamics during stress. *Molecular and Cellular Biology*, *34*(5), 807–819. https://doi.org/10.1128/MCB.01483-13

Schade, A. E., Fischer, M., & DeCaprio, J. A. (2019). RB, p130 and p107 differentially repress G1/S and G2/M genes after p53 activation. *Nucleic Acids Research*, *47*(21), 11197–11208. https://doi.org/10.1093/nar/gkz961

Scimè, A., Grenier, G., Huh, M. S., Gillespie, M. A., Bevilacqua, L., Harper, M.-E., & Rudnicki, M. A. (2005). Rb and p107 regulate preadipocyte differentiation into white versus brown fat through repression of PGC-1α *Cell Metabolism*, *2*(5), 283–295. https://doi.org/10.1016/j.cmet.2005.10.002

Scimè, A., Soleimani, V. D., Bentzinger, C. F., Gillespie, M. A., Grand, F. Le, Grenier, G., Bevilacqua, L., Harper, M.-E., & Rudnicki, M. A. (2010). Oxidative status of muscle is determined by p107 regulation of PGC-1α. *Journal of Cell Biology*, *190*(4), 651–662. https://doi.org/10.1083/jcb.201005076

Seale, P., Sabourin, L. A., Girgis-Gabardo, A., Mansouri, A., Gruss, P., & Rudnicki, M. A. (2000). Pax7 Is Required for the Specification of Myogenic Satellite Cells. *Cell*, *102*(6), 777–786. https://doi.org/10.1016/S0092-8674(00)00066-0

Seyer, P., Grandemange, S., Busson, M., Carazo, A., Gamaléri, F., Pessemesse, L., Casas, F., Cabello, G., & Wrutniak-Cabello, C. (2006). Mitochondrial activity regulates myoblast differentiation by control of c-Myc expression. *Journal of Cellular Physiology*, *207*(1), 75–86. https://doi.org/10.1002/jcp.20539

Seyer, P., Grandemange, S., Rochard, P., Busson, M., Pessemesse, L., Casas, F., Cabello, G., & Wrutniak-Cabello, C. (2011). P43-dependent mitochondrial activity regulates myoblast differentiation and slow myosin isoform expression by control of Calcineurin expression. *Experimental Cell Research*, *317*(14), 2059–2071. https://doi.org/10.1016/j.yexcr.2011.05.020

Shah, V. (2023). *A ROLE FOR p107 IN MUSCLE SATELLITE CELL SELF-RENEWAL* (Master's thesis). Available from York Electronic Theses and Dissertations.

Sin, J., Andres, A. M., Taylor, D. J. R., Weston, T., Hiraumi, Y., Stotland, A., Kim, B. J., Huang, C., Doran, K. S., & Gottlieb, R. A. (2016). Mitophagy is required for mitochondrial biogenesis and myogenic differentiation of C2C12 myoblasts. *Autophagy*, *12*(2), 369–380. https://doi.org/10.1080/15548627.2015.1115172

Sincennes, M.-C., Brun, C. E., Lin, A. Y. T., Rosembert, T., Datzkiw, D., Saber, J., Ming, H., Kawabe, Y., & Rudnicki, M. A. (2021). Acetylation of PAX7 controls muscle stem cell self-renewal and differentiation potential in mice. *Nature Communications*, *12*(1), 3253. https://doi.org/10.1038/s41467-021-23577-z

Song, S. B., & Hwang, E. S. (2019). A Rise in ATP, ROS, and Mitochondrial Content upon Glucose Withdrawal Correlates with a Dysregulated Mitochondria Turnover Mediated by the Activation of the Protein Deacetylase SIRT1. In *Cells* (Vol. 8, Issue 1). https://doi.org/10.3390/cells8010011

Song, Z., Chen, H., Fiket, M., Alexander, C., & Chan, D. C. (2007). OPA1 processing controls mitochondrial fusion and is regulated by mRNA splicing, membrane potential, and Yme1L. *The Journal of Cell Biology*, *178*(5), 749–755. https://doi.org/10.1083/jcb.200704110

Sousa-Victor, P., García-Prat, L., & Muñoz-Cánoves, P. (2022). Control of satellite cell function in muscle regeneration and its disruption in ageing. *Nature Reviews Molecular Cell Biology*, *23*(3), 204–226. https://doi.org/10.1038/s41580-021-00421-2

Tang, A. H., & Rando, T. A. (2014). Induction of autophagy supports the bioenergetic demands of quiescent muscle stem cell activation. *The EMBO Journal*, *33*(23), 2782–2797. https://doi.org/10.15252/embj.201488278

Tieland, M., Trouwborst, I., & Clark, B. C. (2018). Skeletal muscle performance and ageing. *Journal of Cachexia, Sarcopenia and Muscle*, *9*(1), 3–19. https://doi.org/https://doi.org/10.1002/jcsm.12238

Tilokani, L., Nagashima, S., Paupe, V., & Prudent, J. (2018). Mitochondrial dynamics: overview of molecular mechanisms. *Essays in Biochemistry*, *62*(3), 341–360. https://doi.org/10.1042/EBC20170104

Tondera, D., Grandemange, S., Jourdain, A., Karbowski, M., Mattenberger, Y., Herzig, S., Da Cruz, S., Clerc, P., Raschke, I., Merkwirth, C., Ehses, S., Krause, F., Chan, D. C., Alexander, C., Bauer, C., Youle, R., Langer, T., & Martinou, J.-C. (2009). SLP-2 is required for stress-induced mitochondrial hyperfusion. *The EMBO Journal*, *28*(11), 1589–1600. https://doi.org/10.1038/emboj.2009.89

van Velthoven, C. T. J., & Rando, T. A. (2019). Stem Cell Quiescence: Dynamism, Restraint, and Cellular Idling. *Cell Stem Cell*, *24*(2), 213–225. https://doi.org/10.1016/j.stem.2019.01.001

Waterham, H. R., Koster, J., van Roermund, C. W. T., Mooyer, P. A. W., Wanders, R. J. A., & Leonard, J. V. (2007). A Lethal Defect of Mitochondrial and Peroxisomal Fission. *New England Journal of Medicine*, *356*(17), 1736–1741. https://doi.org/10.1056/NEJMoa064436

Weckmann, K., Diefenthäler, P., Baeken, M. W., Yusifli, K., Turck, C. W., Asara, J. M., Behl, C., & Hajieva, P. (2018). Metabolomics profiling reveals differential adaptation of major energy metabolism pathways associated with autophagy upon oxygen and glucose reduction. *Scientific Reports*, *8*(1), 2337. https://doi.org/10.1038/s41598-018-19421-y

Westerberg, G., Chiesa, J. A., Andersen, C. A., Diamanti, D., Magnoni, L., Pollio, G., Darpo, B., & Zhou, M. (2015). Safety, pharmacokinetics, pharmacogenomics and QT concentration-effect modelling of the SirT1 inhibitor selisistat in healthy volunteers. *British Journal of Clinical Pharmacology*, *79*(3), 477–491. https://doi.org/10.1111/bcp.12513

Wirt, S. E., & Sage, J. (2010). p107 in the public eye: an Rb understudy and more. *Cell Division*, *5*, 9. https://doi.org/10.1186/1747-1028-5-9

Xiao, Z. X., Ginsberg, D., Ewen, M., & Livingston, D. M. (1996). Regulation of the retinoblastoma protein-related protein p107 by G1 cyclin-associated kinases. *Proceedings of the National Academy of Sciences*, *93*(10), 4633–4637. https://doi.org/10.1073/pnas.93.10.4633

Yang, Y., & Sauve, A. A. (2016). NAD(+) metabolism: Bioenergetics, signaling and manipulation for therapy. *Biochimica et Biophysica Acta*, *1864*(12), 1787–1800. https://doi.org/10.1016/j.bbapap.2016.06.014

Yartseva, V., Goldstein, L. D., Rodman, J., Kates, L., Chen, M. Z., Chen, Y.-J. J., Foreman, O., Siebel, C. W., Modrusan, Z., Peterson, A. S., & Jovičić, A. (2020). Heterogeneity of Satellite Cells Implicates DELTA1/NOTCH2 Signaling in Self-Renewal. *Cell Reports*, *30*(5), 1491-1503.e6. https://doi.org/10.1016/j.celrep.2019.12.100

Yin, H., Price, F., & Rudnicki, M. A. (2013). Satellite cells and the muscle stem cell niche. *Physiological Reviews*, *93*(1), 23–67. https://doi.org/10.1152/physrev.00043.2011

Zammit, P. S. (2017). Function of the myogenic regulatory factors Myf5, MyoD, Myogenin and MRF4 in skeletal muscle, satellite cells and regenerative myogenesis. *Seminars in Cell & Developmental Biology*, *72*, 19–32. https://doi.org/https://doi.org/10.1016/j.semcdb.2017.11.011

Zhang, J., Hua, C., Zhang, Y., Wei, P., Tu, Y., & Wei, T. (2020). KAP1-associated transcriptional inhibitory complex regulates C2C12 myoblasts differentiation and mitochondrial biogenesis via miR-133a repression. *Cell Death & Disease*, *11*(9), 732. https://doi.org/10.1038/s41419-020-02937-5

Zhu, L., Harlow, E., & Dynlacht, B. D. (1995). p107 uses a p21CIP1-related domain to bind cyclin/cdk2 and regulate interactions with E2F. *Genes & Development*, *9*(14), 1740–1752. https://doi.org/10.1101/gad.9.14.1740